



HAL
open science

Cold Tectonics of Kos, Central Dodecanese: Oligocene Bivergent Extension of the Pelagonian Domain

Vincent Roche, Bernhard Grasemann, David Schneider, Konstantinos Soukis,
Michael Pichler

► **To cite this version:**

Vincent Roche, Bernhard Grasemann, David Schneider, Konstantinos Soukis, Michael Pichler. Cold Tectonics of Kos, Central Dodecanese: Oligocene Bivergent Extension of the Pelagonian Domain. *Tectonics*, 2024, 43 (12), 10.1029/2024TC008355 . hal-04843173

HAL Id: hal-04843173

<https://hal.science/hal-04843173v1>

Submitted on 17 Dec 2024

HAL is a multi-disciplinary open access archive for the deposit and dissemination of scientific research documents, whether they are published or not. The documents may come from teaching and research institutions in France or abroad, or from public or private research centers.

L'archive ouverte pluridisciplinaire **HAL**, est destinée au dépôt et à la diffusion de documents scientifiques de niveau recherche, publiés ou non, émanant des établissements d'enseignement et de recherche français ou étrangers, des laboratoires publics ou privés.



Distributed under a Creative Commons Attribution 4.0 International License

Cold Tectonics of Kos, Central Dodecanese: Oligocene Bivergent Extension of the Pelagonian Domain

Vincent Roche^{1,2} , Bernhard Grasemann³ , David Schneider⁴ , Konstantinos Soukis⁵ , and Michael Pichler³

¹Laboratoire de Planétologie et Géosciences, LPG UMR 6112, CNRS, Le Mans Université, Univ Angers, Nantes Université, Le Mans, France, ²Institut des Sciences de la Terre Paris, Sorbonne Université, Paris, France, ³Department of Geology, University of Vienna, Vienna, Austria, ⁴Department of Earth and Environmental Sciences, University of Ottawa, Ottawa, ON, Canada, ⁵Faculty of Geology and Geoenvironment, National and Kapodistrian University of Athens, Athens, Greece

Key Points:

- All units from Kos belong to the Pelagonian domain
- Post-orogenic N-S bivergent extension started in the Oligocene in the Pelagonian domain
- Mid-Neogene to recent extension related to slab retreat and tearing maintains a constant N-S direction

Supporting Information:

Supporting Information may be found in the online version of this article.

Correspondence to:

V. Roche,
vincent.roche@univ-lemans.fr

Citation:

Roche, V., Grasemann, B., Schneider, D., Soukis, K., & Pichler, M. (2024). Cold tectonics of Kos, central Dodecanese: Oligocene bivergent extension of the Pelagonian domain. *Tectonics*, 43, e2024TC008355. <https://doi.org/10.1029/2024TC008355>

Received 4 APR 2024
Accepted 7 NOV 2024

Author Contributions:

Conceptualization: Vincent Roche, Bernhard Grasemann, David Schneider, Konstantinos Soukis

Funding acquisition: Vincent Roche, Bernhard Grasemann, David Schneider

Methodology: Vincent Roche, Bernhard Grasemann, David Schneider, Konstantinos Soukis, Michael Pichler

Writing – original draft: Vincent Roche, Bernhard Grasemann, David Schneider, Konstantinos Soukis

Abstract Tectonic and lithological correlations between the Cycladic Blueschist Unit of the Aegean domain and Pelagonian domain of the western Turkey have rarely been proposed. Herein, we focus on the pre-volcanic geology of Kos, and investigate the tectonic history of the central Dodecanese Islands and the general correlation between the two domains. Raman Spectroscopy of Carbonaceous Material analyses combined with white mica ⁴⁰Ar/³⁹Ar and zircon (U-Th)/He geochronology were carried out to determine peak temperatures and the timing of tectonothermal events recorded by the various units. Three tectonic units were identified: (a) the Dikeos Unit including the Paleozoic Unit overlain by the Permo-Triassic Wildflysch Unit, whose rocks have reached a maximum temperature of 300°C; (b) the Marina Basement Unit was thrust onto the Dikeos Unit with top-to-N kinematics during the Paleocene, reaching a maximum temperature of 565°C; (c) the Marina Cover Unit is preserved as isolated klippen juxtaposed onto the Dikeos Unit along the Oligocene top-to-SSE Kos Detachment. The Dikeos Unit was then intruded by a c. 10 Ma monzonite, creating a few hundred meters wide metamorphic aureole. At the regional scale, we propose that units from Kos belong to the Pelagonian domain and that post-orogenic N-S bivergent extension started in the Oligocene. Over the same time, the deformation started to propagate to deeper structural levels affecting the rocks of the Cycladic Blueschist Unit. Unfortunately, the lack of consensus on the deformation history in southwestern Turkey does not unequivocally allow the constraints to be extended eastward. Finally, mid-Neogene to recent extension continues within a consistent N-S direction, which is related to slab retreat and tearing.

1. Introduction

The eastern Mediterranean region recorded continuous subduction of the lithosphere beneath Eurasia since the Cretaceous period, leading to the formation of the Hellenide and Tauride orogens (Bonneau, 1984; Brun & Faccenna, 2008; Jacobshagen et al., 1978; van Hinsbergen et al., 2005). Crustal extension within the eastern Mediterranean region started in the late Eocene and continues to the present day (e.g., Jolivet and Brun, 2010), affecting the various nappe sequences that originated from distinct paleogeographic settings. Depending on the tectonic evolution, rocks recorded different tectonometamorphic histories that are characterized by syn-orogenic exhumation overprinted by post-orogenic extensional processes to varying extents (Jolivet and Brun, 2010; Ring et al., 2010), making global correlations challenging (e.g., Grasemann et al., 2022a; Jolivet et al., 2004; Ring et al., 1999; Roche et al., 2019). Although the kinematics in the region have been mainly controlled by the southward retreat and the tearing of the African slab under the Mendere Massif (e.g., Dilek & Altunkaynak, 2009; Jolivet et al., 2013; Roche et al., 2019) as imaged by tomographic models (e.g., Berk Biryol et al., 2011; De Boorder et al., 1998; Piromallo & Morelli, 2003; Salaün et al., 2012), crustal deformation related to post-orogenic processes follows a consistent symmetrical pattern in Cyclades and Mendere Massif (Figure 1).

In the Cyclades, extension occurred with the generation of several crustal-scale detachment fault systems (i.e., detachments; Lister et al., 1984) during the late Oligocene to early Miocene (e.g., Grasemann et al., 2012; Jolivet et al., 2010; Ring et al., 2010). The main ductile shear direction was top-to-NNE in the northern part of the Cyclades (e.g., Tinos, Andros, Jolivet et al., 2010) and top-to-SSW to -SSE in its southern part (e.g., Kea, Kythnos, Serifos, Santorini, Amorgos, Grasemann et al., 2012; Schneider et al., 2018, Laskari et al., 2024; Figure 1). During the mid-Miocene, several metamorphic core complexes were then exhumed in the back-arc region of the Hellenic subduction zone (e.g., Gautier et al., 1993; Jolivet et al., 2004; Lister et al., 1984; Urai

© 2024. The Author(s).

This is an open access article under the terms of the [Creative Commons Attribution License](https://creativecommons.org/licenses/by/4.0/), which permits use, distribution and reproduction in any medium, provided the original work is properly cited.

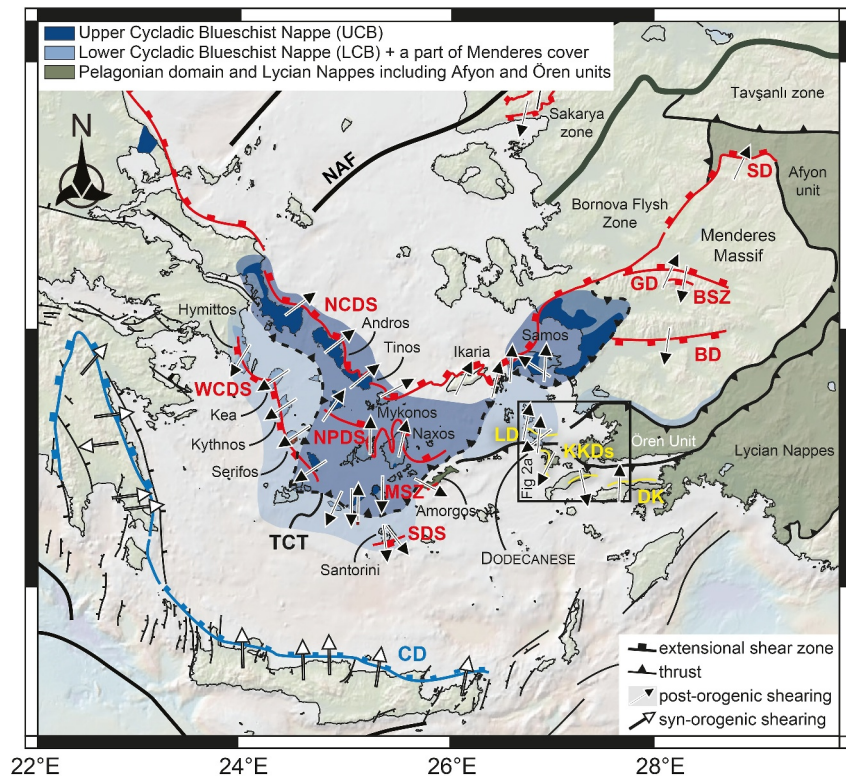


Figure 1. Simplified tectonic map of the Aegean region modified from Grasemann et al. (2022a) showing kinematics of major faults during slab roll back. Note that the red and blue lines correspond to post- and syn-orogenic extensional detachment, respectively. BD = Büyük Menderes Detachment, CD = Cretan Detachment, DK = Datça–Kale fault, GD = Gediz Menderes Detachment, KKDS = Kalymnos-Kos Detachment System, LD = Leros Detachment, MSZ = Mousros Shear Zone, NAF = North Anatolian Fault, NCDS = North Cycladic Detachment System, NPDS = Naxos-Paros, Detachment System, SD = Simav Detachment, SDS = Santorini Detachment System, TCT = Trans-Cycladic Thrust, and WCDS = West Cycladic Detachment System.

et al., 1990). The kinematics of deformation remained unchanged, showing a predominant top-to-NE or -N shear direction on the islands of Mykonos, Naxos, and Ikaria (Jolivet et al., 2013), and top-to-SW on Hymittos (Coleman et al., 2020) and Serifos (Grasemann et al., 2012; Figure 1). Interestingly, the early detachments (i.e., Oligocene to early Miocene) have been reactivated or continued to accommodate extension as shown by some zircon (U-Th)/He ages and brittle deformation markers that overprinted ductile deformation (e.g., Santorini, Schneider et al., 2018). In western Anatolia, the Menderes core complex was exhumed in two main stages (Gessner et al., 2013; Ring et al., 2003) by several low-angle normal faults. The Simav Detachment is located in the northern part of Menderes Massif and shows a consistent top-to-NNE sense of shear (e.g., Bozkurt et al., 2011; Işık & Tekeli, 2001) whereas deformation related to the Büyük Menderes Detachment displays an opposing sense of shear (e.g., Hetzel et al., 1995; Lips et al., 2001; Figure 1). Both detachments began in the Oligo-Miocene (e.g., Bozkurt et al., 2011; Seyitoğlu et al., 2004), whereas the second stage occurred during the mid-Miocene along the Alaşehir and the Bozdag shear zone and deformation is bivergent—that is top-to-N and -S (Figure 1). Similar to the Cyclades, the early detachments have been reactivated at brittle structural levels (e.g., Hetzel et al., 2013).

In the transition between the Aegean and Anatolian plates, few studies have considered the kinematics of deformation. Roche et al. (2019) proposed that post-orogenic deformation in the northern part of the Dodecanese Islands was predominantly asymmetric and accommodated along top-to-NNE detachments (Figure 2a), except locally on Samos where E-W extension could reflect the existence of the sinistral wrench system in the early/mid-Miocene (Ring et al., 2017). However, the recent work of Grasemann et al. (2022a) on Kalymnos revealed that extension is also accommodated by the top-to-SSW Kalymnos Detachment (Figure 2a). The detachment started in the late Oligocene in the Pelagonian domain, implying that extension is bivergent at the scale of the Aegean and Anatolian transition zone. This Oligocene activity is confirmed by relatively old fission track ages, suggesting

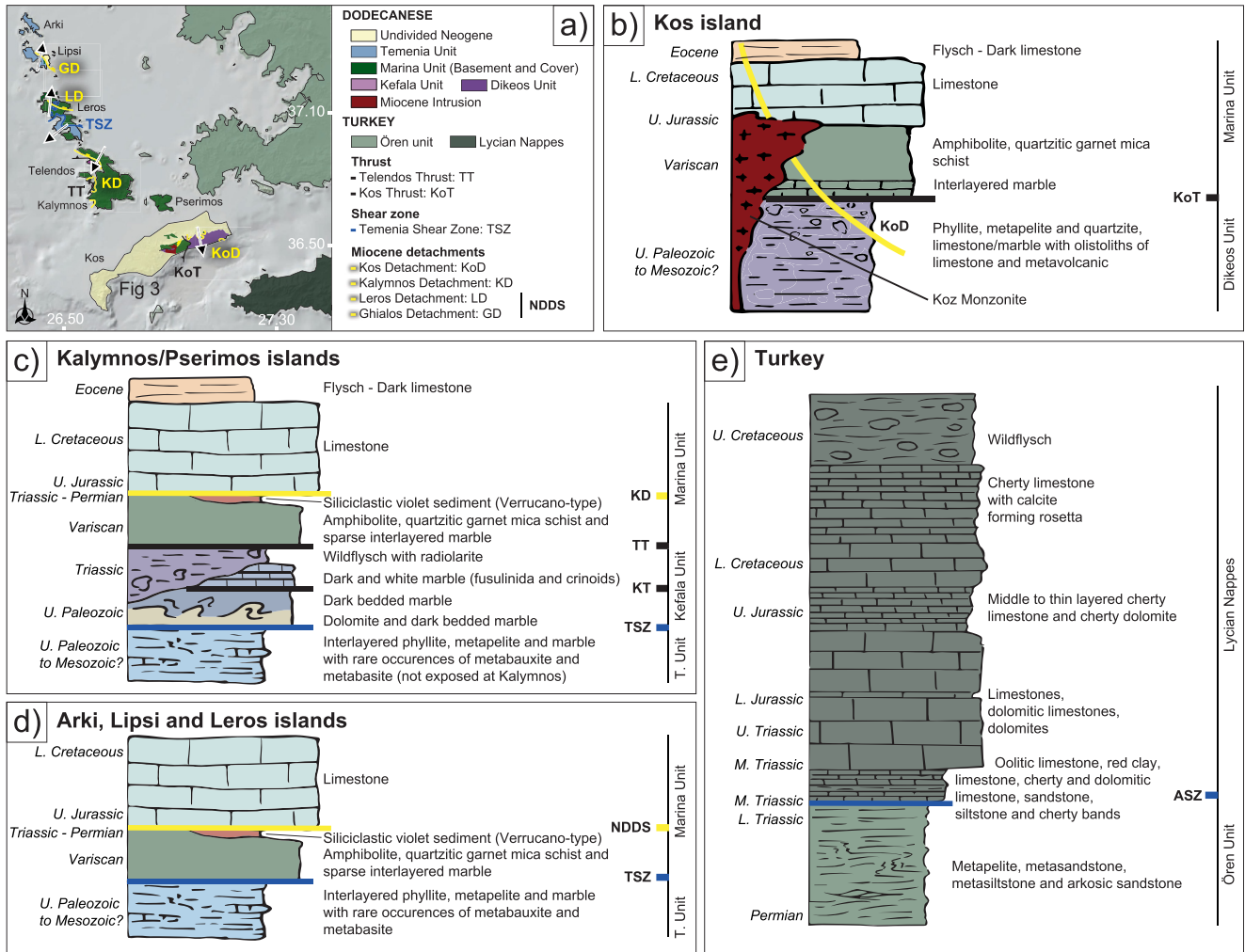


Figure 2. (a) Tectonic and geological map of the Dodecanese region. Arrows indicate the sense of post-orogenic shearing. Simplified tectono-stratigraphic sequences modified from Grasemann et al. (2022a) from (b) Kos, (c) Kalymnos, (d) the Dodecanese Islands and (e) Turkey. ASZ = Akçakaya Shear Zone, KT = Kefala Thrust, NDDS = North Dodecanese Detachments System, T = Temenia (unit). Note that ASZ and KT are not present in panel (a).

that mid to late Miocene deformation is heterogeneous (Ring et al., 2017). Nonetheless, further south, the tectonics on Kos remain enigmatic because the island is partly covered by the easternmost magmatic complex of the South Aegean volcanic arc (Bachmann et al., 2019; Pe-Piper et al., 2005). A few studies have proposed the existence of a relatively isolated late Miocene brittle top-to-N detachment (van Hinsbergen and Boekhout, 2009) or an Alpine thrust between the two main units on the island (Papanikolaou and Nomikou, 1998). A recent study by Soder et al. (2016) also reported several NNE-to-NNW striking lamprophyre dikes. The latter post-date the coarse grained Kos monzonite which is dated at 9–12 Ma (Altherr et al., 1976; Henjes-Kunst et al., 1988). The synchronicity of the deep-seated magmatism and the shallow crustal extension is peculiar and necessitates further investigation.

In this paper, we extend the previous work of Grasemann et al. (2022a), to focus on Kos, where structural interpretations differ. For example, the two main units (i.e., Wildflysch and Paleozoic units) are either separated by an Alpine thrust (Papanikolaou and Nomikou, 1998), or by the late Miocene top-to-N Kos Detachment (van Hinsbergen and Boekhout, 2009). In addition, lithological correlations are not straightforward. Based on lithology, age and tectonostratigraphic framework, Kos units may either belong to the tectonostratigraphically lowest Aegean nappes (i.e., the Basal Unit, the Gavrovo-Tripolitza Unit, the Phyllite-Quartzite Unit; Papanikolaou and Nomikou, 1998) or to the structurally highest Lycian Nappes (van Hinsbergen and Boekhout, 2009). We show that rock units on Kos can be correlated with the units on Kalymnos and belong to the Pelagonian domain. Our

new thermal, geochronological and structural data indicate two main stages related to post-orogenic extension: (a) a N-S bivergent extension accommodated by several detachments that started in the Oligocene in the north-central Dodecanese Islands and (b) a youngest N-S increment which post-dated the late Miocene Kos monzonite intrusion. In addition, we propose that the top-to-N Kos Thrust is similar to Telendos Thrust on Kalymnos (Grasemann et al., 2022a), juxtaposing the Marina Basement onto the Dikeos Unit during the Paleocene. The connections between these different units will provide constraints on the subduction dynamics of the Aegean-Anatolian domain.

2. Geological Setting of the Aegean-Anatolian Domain

The initial investigation by Franz et al. (2005) combined with the recent works of Roche et al. (2018, 2019) and Grasemann et al. (2022a) highlight the bedrock geology of the northern Dodecanese Islands (Figure 2a). Two main units—the Pelagonian Unit that it is part of the Pelagonian domain and the Temenia Unit—have been recognized, separated by the top-to-NE Temenia Shear Zone (Roche et al., 2018). The Pelagonian domain covers most of the northern Dodecanese Islands, and consists mainly of a Paleozoic basement (i.e., Marina Basement Unit) covered by an upper Paleozoic limestone and wildflysch Unit (i.e., Kefala Unit) and/or by a Mesozoic platform sequence (i.e., Marina Cover; Figures 2c and 2d). The Marina Basement Unit is Variscan amphibolite facies rocks including garnet mica schists, amphibolites and quartzites. The Kefala Unit is part of the structurally highest Pelagonian domain and is exposed on the Kalymnos archipelago (Grasemann et al., 2022a). It consists of imbricated and folded Upper Paleozoic fossil-rich limestones sealed by a wildflysch containing marble and ultramafic blocks. The Marina Cover comprises violet shales (Verrucano-type Formation) topped by Mesozoic unmetamorphosed limestones. Units originating from the Pelagonian domain are also found in continental Greece, Crete, and in the Cyclades overlying the detachments (e.g., Bonneau, 1984; Papanikolaou, 2013; Patzak et al., 1994). The Temenia Unit occurs in the northern Dodecanese, on the Islands of Leros, Lipsi and Arki (Figure 2a). This unit is made of probable Upper Paleozoic to Mesozoic sediments including lenses of basic rocks (Figure 2d), and has been buried to at least 20 km depth along a cold metamorphic gradient (Roche et al., 2018). Roche et al. (2019) proposed to correlate this unit with the lower part of the Cycladic Blueschist Nappe, which records mainly Eocene blueschist facies metamorphism compared to the eclogite facies observed in upper structural levels (cf. Grasemann et al., 2018). The Cycladic Blueschist Nappe is exposed on most of the Cycladic islands (Figure 1) and is dominated by a schist-marble series including metabasites interleaved with metatuffs and metapelites. A part of this unit experienced a high-temperature overprint reaching amphibolite facies conditions during the late Oligocene to early Miocene (e.g., Altherr et al., 1982; Bröcker et al., 2013; Parra et al., 2002; Wijbrans and McDougall, 1988).

In the Aegean domain, two other units are found in the external zones of the Hellenides. Below the Cycladic Blueschist Unit, the Basal Unit considered as the low grade metamorphosed equivalent of the Gavrovo-Tripolitza Unit (Bonneau, 1984; Papanikolaou, 2021) with evidence of late Eocene to Oligocene high-pressure, low-temperature parageneses, is exposed as tectonic windows (e.g., Olympos, Ossa, Almyropotamos; e.g., Godfriaux & Pichon, 1980; Godfriaux & Ricou, 1991; Shaked et al., 2000; Ducharme et al., 2022). The Basal Unit is defined by a thick sequence of carbonates ranging from the Triassic to the Eocene, topped by a Upper Eocene to Lower Oligocene metaflysch (e.g., Papanikolaou, 2021; Ring et al., 2001). The second unit is the Phyllite-Quartzite Unit, observed in the Peloponnese and Crete that was exhumed beneath the Gavrovo-Tripolitza Unit by the Cretan Detachment, active during the Miocene (Fassoulas et al., 1994; Grasemann et al., 2019; Jolivet et al., 1996; Ring et al., 2001). The unit is composed of continental to shallow marine siliciclastics and impure carbonates interlayered with Upper Permian-Upper Triassic volcanites (Creutzburg et al., 1977; Hall et al., 1984; Krahl et al., 1983). The Phyllite-Quartzite Unit has been metamorphosed under high-pressure and low-temperature conditions with a peak of metamorphism around 16 kbar and 400°C on western Crete (Jolivet et al., 1996).

In the Anatolian domain, the Lycian Nappes are the Turkish equivalent of the Pelagonian and cover a large area in western Turkey (Figures 1 and 2a). The nappes are Mesozoic unmetamorphosed limestones including dolomites and cherty limestones topped by Upper Cretaceous wildflysch (Figure 2e; Rimmelé et al., 2003). The nappes were emplaced southeastward onto the continental margin during the latest Cretaceous and Eocene (Collins & Robertson, 1997). Paradoxically, the deeper structural levels record a high-pressure metamorphic event associated with top-to-NE shearing (Rimmelé et al., 2003, 2005) during the early Paleocene (Pourteau et al., 2013).

Located below the Lycian Nappes, the Menderes Massif is a tectonic window exposing metamorphic rocks that were derived from the central Anatolide-Tauride continental block. Ring et al. (1999) and Gessner, Piazzolo, et al. (2001) presented the Menderes Massif as a stack of nappes formed during the early Paleozoic to Tertiary, and consisting of a series of crystalline Pan-African basement and Mesozoic carbonate units that underwent a complex orogenic history. The nappe stack was then reworked and exhumed along several detachments during the Miocene (Gessner, Ring, et al., 2001; Hetzel et al., 1995).

3. Geology of Kos

The island of Kos in the central Dodecanese belongs to volcanic field, which is the easternmost magmatic complex of the South Aegean volcanic arc (Bachmann et al., 2019; Pe-Piper et al., 2005). The basement geology of Kos is characterized by Paleozoic to Paleogene marine metasediments, which are intruded by a Miocene pluton exposed predominantly in the eastern parts of the island (Altherr et al., 1976; Keller, 1969; Willmann, 1983). The central and western parts (Kefalos peninsula) of Kos are dominated by Upper Miocene to Quaternary marine to lacustrine sediments that are often overlain by Pliocene to Pleistocene volcanoclastic deposits with isolated Mesozoic limestone blocks (Allen et al., 1999; Willmann, 1983). The main source of these volcanoclastic sediments results from the 161 ka Kos Plateau Tuff eruption, which represents the largest Quaternary eruption from volcanic centers in the Aegean region (Smith et al., 1996).

Here, we focus on the Paleozoic - Eocene rocks exposed in the southeastern part of the island in the Dikeos massif (also Dicheo massif in the literature), which in its western half consists of fossiliferous Ordovician-Carboniferous metapelite, marble, quartzite, phyllite, and meta-conglomerate (Paleozoic Unit) that reveal deformation under low grade metamorphic conditions (Altherr et al., 1976; Desio, 1931; Papanikolaou and Nomikou, 1998). The eastern part of the massif is dominated by metapelites, quartzites and phyllites with large (300 m) olistoliths of meta-dolostone, marble and metavolcanic rocks (Wildflysch Unit) of either unknown stratigraphic position (Altherr et al., 1976; Desio, 1931), or Mesozoic (Papanikolaou and Nomikou, 1998) to Paleogene in age (van Hinsbergen and Boekhout, 2009). According to Papanikolaou and Nomikou (1998), the Wildflysch Unit was thrust to the west on top of the Paleozoic Unit. Alternatively, van Hinsbergen and Boekhout (2009) suggest that the contact between the Paleozoic and Wildflysch units is the late Miocene top-to-N Kos Detachment.

The Paleozoic Unit together with the Wildflysch Unit are tectonically overlain by Mesozoic limestone klippen either along a thrust (Altherr et al., 1976; Papanikolaou and Nomikou, 1998) or along a detachment fault (i.e., Kos Detachment; van Hinsbergen and Boekhout, 2009). The unmetamorphosed thick-bedded micritic limestones and dolomitic limestones with cherts are locally overlain by Eocene nummulitic limestones and flysch (Desio, 1931). Papanikolaou and Nomikou (1998) correlated the purported Mesozoic sequences to Paleogene klippen above the Tripolitza and Pindos nappes. Alternatively, these rocks could represent the western extension of the Turkish Lycian nappes (van Hinsbergen and Boekhout, 2009).

The western part of the Dikeos massif was intruded by the coarse grained Kos monzonite at 9–12 Ma (Altherr et al., 1976; Henjes-Kunst et al., 1988) at a depth corresponding to 0.3–0.5 GPa (Kalt et al., 1998). Biotite K-Ar dates are c. 9.5 Ma and titanite fission track ages are c. 8.5 Ma, indicative of rapid cooling of the intrusion (Altherr et al., 1982). The intrusion produced an indelible contact metamorphic signature in the Ordovician-Carboniferous host rocks with temperatures of ~800°C at the contact to ~500°C at a distance of several kilometers (Altherr et al., 1976; Kalt et al., 1998). Kalt et al. (1998) mapped isograds that they interpreted to be a metamorphic aureole decreasing away from the intrusive contact. They recognized wollastonite, sillimanite, diopside, cordierite, to biotite + muscovite in the eastern part of the massif. The absence of contact metamorphism in the Mesozoic to Paleogene klippen, which partly overlies the granitoid, has been used as an important argument to infer that this contact is either a thrust (Altherr et al., 1976; Papanikolaou and Nomikou, 1998) or a detachment fault (van Hinsbergen and Boekhout, 2009).

4. Revised Map and Tectonostratigraphy of the Paleozoic to Neogene Rocks

With only very minor modifications of the excellent geological map of Kos (Triantaphyllis and Mavrides, 1998), we present our field observations, in which we suggest a new tectonostratigraphy of the Paleozoic to Neogene rocks on Kos (Figures 3 and 4). We propose three major differences in the tectonostratigraphy: (a) Instead of a tectonic contact (Papanikolaou and Nomikou, 1998; van Hinsbergen and Boekhout, 2009), we mapped a depositional contact of the Paleozoic Unit with the overlying Permo-Triassic Wildflysch Unit, and thus decided to

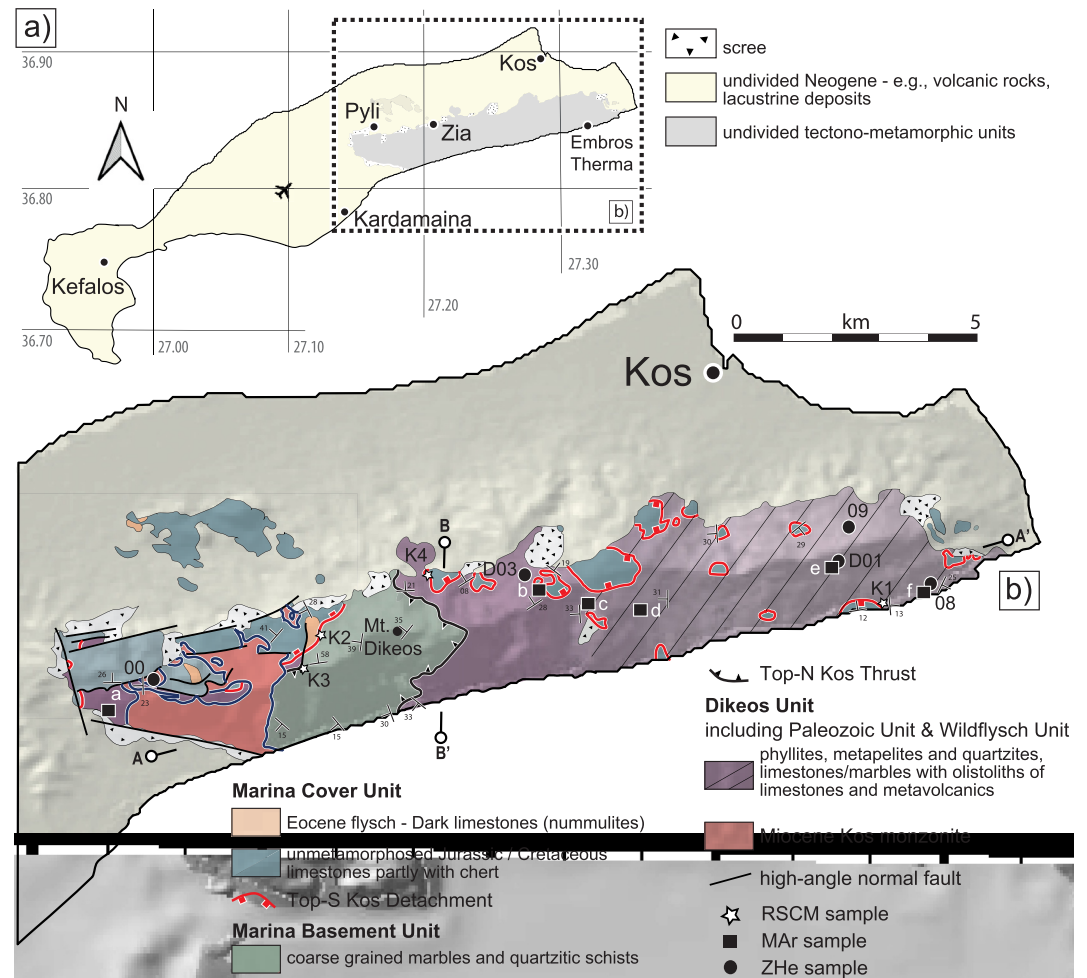


Figure 3. Simplified geological map of Kos, modified after Triantaphyllis and Mavrides (1998). Structural profiles A-A' and B-B' are in Figure 4. Note that the violet and cross-hatched area corresponds to the Wildflysch Unit.

group these two units together as the Dikeos Unit. (b) In contrast to the proposed intrusive contact metamorphic overprint (Kalt et al., 1998), which only extends a few hundred meters from the monzonite intrusive contact, we introduce a new higher grade unit that is thrust onto the low grade Paleozoic Unit with top-to-N kinematics. (c) We redefined and remapped the Kos Detachment below the unmetamorphosed Mesozoic limestones, which has top-to-S kinematics instead of the suggested top-to-N shear sense (van Hinsbergen and Boekhout, 2009).

4.1. Dikeos Unit (Including the Paleozoic Unit and Wildflysch Unit)

The lowermost unit on Kos, the Dikeos Unit, consists of low grade Paleozoic metasediment comprised mainly of bedded metasandstone, metaarkosic sandstone, metapelite and subordinate impure marble layers and bedded meta-chert (Figure 5a). Chaotic polymictic conglomerate (Figure 5b) and large blocks of metavolcanite, dolomitic limestone and marble up to ~300 m in diameter occur in the east. There is a gradational transition between the Paleozoic Unit (without olistoliths) and the Wildflysch Unit (with increasing numbers of conglomerate layers and olistoliths toward the east) and no tectonic contact between the two has been observed. The entire package was metamorphosed under lower greenschist facies conditions.

Most of the preserved sedimentary bedding dips generally toward the SW to NW with some dipping in the opposite direction, which is the result of a large-scale open dome along roughly N-S and W-E trending fold axes (pi-circles in dashed gray, Figure 4c). Although most rocks record a second phase of axial plane cleavage, folding at the outcrop scale is rarely observed and restricted to some minor kink-type folding (saxpl2, Figure 5a) or soft sediment deformation (isoclinal upright fold, Figure 5a). The greenschist facies rocks record occasional new

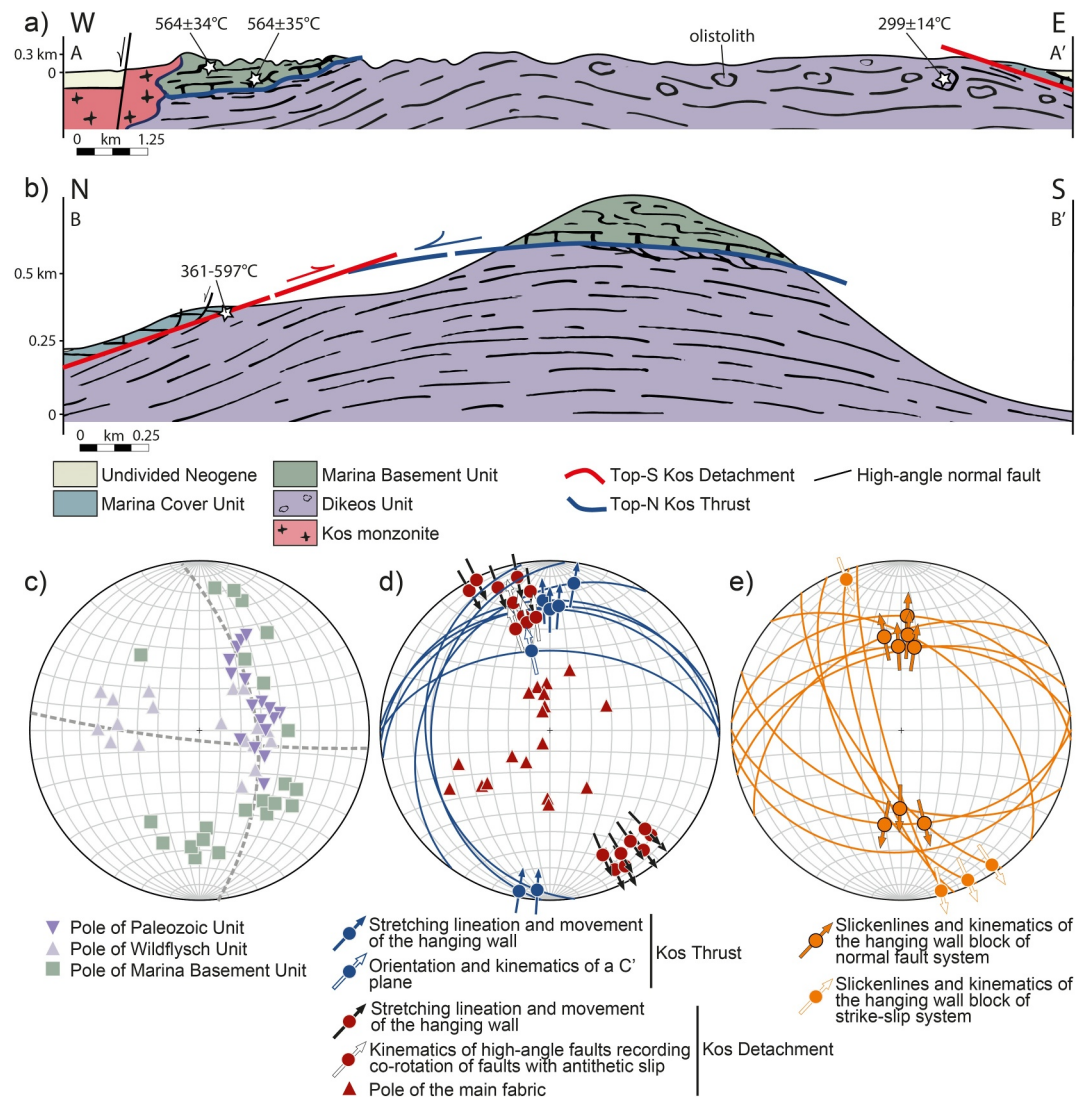


Figure 4. (a) and (b) Geological cross-sections showing the main tectonic contacts between the units. Profiles shown in Figure 3. (c) Poles of the Paleozoic Unit and the Wildflysch Unit show an open dome with roughly N-S and W-E trending fold axes (pi-circles in dashed gray). The higher grade rocks of the Marina Basement Unit follow a similar trend and dip into a northwestern and southeastern direction with a cluster dipping toward the north. (d) Stereographic data showing the orientation of the Kos Thrust (blue great circles) and the kinematics of Kos Thrust and Kos Detachment. (e) Angelier plot of brittle fault plotted as orange great circles. Orange arrows show a conjugate high-angle normal fault system showing N-S extension. White arrows with orange outline show a NNW-SSE striking sinistral strike-slip system.

growth of fine grained biotite along the cleavage planes (S2, Figure 5c) and evidence of dynamic recrystallization of quartz veins by subgrain rotation and bulging, yet most of the deformation is accommodated by dissolution-precipitation and the formation of bedding parallel pressure solution cleavage and oblique axial plane cleavage (Figure 5c). Detrital grains of quartz, feldspar, lithic fragments, and muscovite are preserved in the microlithons between the cleavage domains (white arrow, Figure 5c). It is important to note that in the whole Dikeos Unit, no evidence of ductile shear zones or ductile high strain deformation has been observed, and most sedimentary structures are well preserved, only slightly overprinted by a metamorphic foliation (S1 in Figure 5c).

4.2. Kos Thrust

On the northwestern slopes of Mt. Dikeos (846 m) and ~2.5 km east of the peak, the higher grade, strongly sheared and re-folded metamorphic rocks of the Marina Basement Unit (see below) are thrust onto the low grade

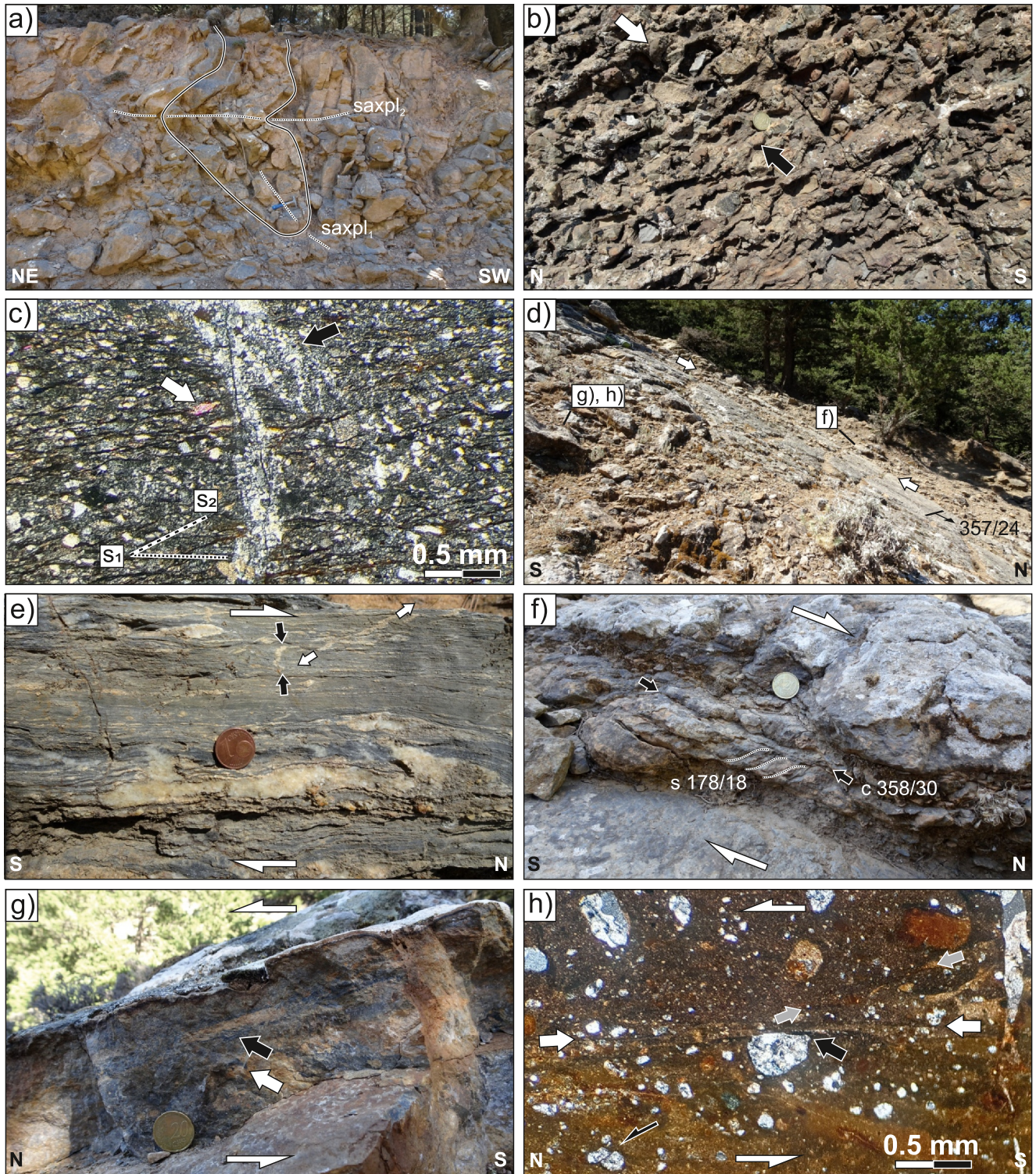


Figure 5.

Dikeos Unit. The thrust zone, with a clear N-S trending stretching lineation, arches over Mt. Dikeos and dips about 25°–30° toward the north on the northern side, and toward the west and southwest on the crest and the southern side of the mountain (Figures 3b and 4d). The thrust is located at the base of a ~300 m thick, white coarse

grained marble layer in fine grained marble mylonites (Figure 5e), which preserves an increasing strain gradient toward the thrust plane. This mylonitic fabric overprints the S1 fabric and may be contemporary with S2 reported in the Dikeos Unit (Figure 5c). Shortened and stretched calcite veins, which have been rotated into the shear direction as well as calcite sigmoids, exhibit a consistent top-to-N shear sense (Figure 5e). Above the thrust plane, the marble mylonites of the Marina Basement Unit are strongly overprinted by an intense SC and SCC' fabric consistent with the top-to-N kinematics (Figure 5f). The thrust is characterized by a 1–2 m thick zone of cohesive ultra-cataclasites with intrusion-like apophyses, which may have been pseudotachylites that have been recrystallized (white arrow, Figure 5g). Except for some SC fabrics (black arrow, Figure 5f), the ultra-cataclasites do not record clear macroscopic shear sense indicators. In thin sections, the ultra-cataclasites contain well-rounded clasts showing no preferred alignment, indicative of rolling and comminution of the clasts (Figure 5h). Almost all of the clasts appear to be derived from metamorphic quartzofeldspathic rocks evincing grain boundary migration, static recrystallization, and partial lattice preferred orientation of the quartz grains, and therefore must be derived from the hanging wall (described below). Some of the quartz clasts are cut by brittle fractures and possess synthetic offsets (black half arrow, Figure 5h). The ultrafine grained matrix is dissected by principal slip surfaces (white arrows, Figure 5h), which separate different generations of ultra-cataclasites and truncate clasts (black arrow). Synthetic Riedel shears (gray arrows, Figure 5h) confirm the top-to-N shear sense.

4.3. Marina Basement Unit

The Marina Basement Unit comprises higher metamorphic grade rocks above the Kos Thrust and mainly consists of coarse grained pure marbles, impure marbles with metachert layers, and metasediments including quartzites and schists. Metamorphic phases are mainly garnets and micas. The main foliation dips steeply toward the north on the northern slopes of Mt. Dikeos, toward the west on the ridge (Figure 6a) and toward SW-SSW along the southern coast (Figure 4c). Internally, the metamorphic rocks record polyphase ductile deformation resulting in Type 2 (mushroom) and Type 3 (hook and crescent) refold structures (Figure 6b). The pure marbles have grain sizes up to 3 mm and exhibit grain boundaries forming triple junctions (black arrow, Figure 6c). The grain boundaries are sutured, and tabular, thick twins (Type II, Ferrill et al., 2004) are partly dynamically crystallized (Type IV, white arrow, Figure 6c). Close to the Kos Thrust the grain size is several orders of magnitude smaller ($<50\ \mu\text{m}$) and preserves a clear shape preferred orientation oblique to the main foliation with consistent top-to-N shear sense criteria (Figure 5f). The partially highly sheared quartzites and mica schists are rich in inter-tectonic garnet, which overgrow an earlier foliation, but form porphyroblasts with strain shadows and strain caps where the mylonitic foliation wraps around the garnets (Figures 6d–6i). Some garnets show two growth stages with an inclusion-poor core and a rim with mostly quartz inclusions (Figures 6d-ii and 6d-iii).

The western side of the Marina Basement Unit is cut by a Miocene monzonite intrusion (see below), creating locally, up to a few hundred meters from the contact, a strong high-temperature metamorphic overprint. The skarns are mainly composed of andradite garnet and pyroxene (hedenbergite, diopside) \pm magnetite (Figure 6e) and either follow the pre-existing foliation in the host rocks or crosscut the fabric as veins or small dikes. Within the contact metamorphic zone, dam-scale mode I cracks cut all structures and are filled with dm-long wollastonite crystals (Figure 6f).

Figure 5. (a) Soft-sediment deformation in marble/bedded-chert layers in the Paleozoic Unit (521904E, 4077747N). The layers are deformed into a hook-shaped Type 3 refold structure with a first fold axis ($1F_1$) 305/20, second fold axis ($1F_2$) 333/15 with an axial plane ($saxpl_2$) 342/15. (b) Polymict meta-conglomerate with marble, dolomite, metavolcanics and chert components in coarse-grained sandy matrix (523600E, 4077536N). Some pebbles are cracked (black arrow) and show solution pits (white arrow). A 20¢ coin is located above the black arrow for scale. (c) Thin section (XPL) photomicrograph of a metaarkosic sandstone showing a bedding parallel pressure solution cleavage (S_1) and an oblique axial plane cleavage (S_2). The detrital grains are mostly quartz, feldspar, lithic fragments and muscovite (marked with a white arrow). Some quartz veins (marked with a black arrow) are deformed by bulging and subgrain rotation recrystallization (513089E, 4075948N). (d) Thrust plane of the Kos Thrust (marked by white arrows) dipping toward north (517654E, 4076451N). Locations of panels (f)–(h) are indicated. (e) Marble ultramylonites above the brittle cataclasites of the Kos Thrust. Shortened/folded (black arrows) and stretched/boudinaged calcite veins indicate top-to-N shear sense (519864E, 4077800N). (f) The cataclasites are strongly overprinted by SC and SCC' fabrics (black arrow) showing a top-to-N kinematics (location in d). (g) Ultra-cataclasites showing possible apophysis of a pseudotachylite (white arrow). Kinematic indicators are rare in these rocks except for some local SC-fabric (black arrow, location in d). (h) Thin section (XPL) photomicrograph of the ultra-cataclasites (location in f) showing an ultrafine-grained matrix with well-rounded clasts of metamorphic quartzites. Black half arrow: quartz clasts cut by brittle fractures with synthetic offsets. White arrow: principal slip surface, which truncates a quartzite clast (black arrow). Gray arrows: synthetic Riedel shears (location in d).

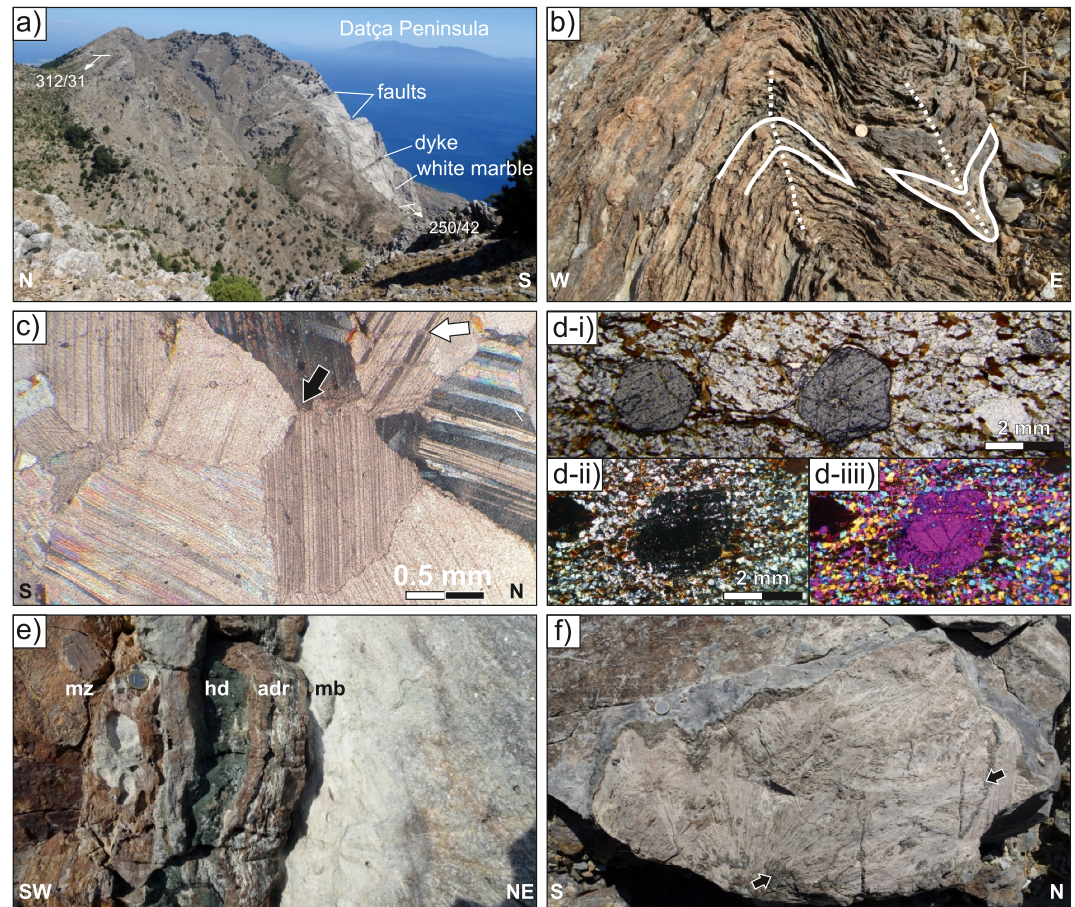


Figure 6. (a) View from the peak of Mt. Dikeos (846 m; 518496E, 4076599N) toward the east showing the NW- to SE-dipping higher grade metamorphic rocks of the Marina Basement Unit. An up to 300 m thick coarse-grained white marble sequence, which is offset by NW-SE striking faults and intruded by volcanic dikes is exposed on the south side of the mountain. (b) Impure layered marble with quartz-rich schists showing Type 2 and Type 3 refold interference patterns. The complex refold structure is cut by the monzonite intrusion, which is 10 m to the left of the picture. Solid white line outlines the trace of the refolded metamorphic layering. Dotted white line indicates the trace of the second fold generation axial surface (516921E, 4074517N). (c) Thin section (XPL) photomicrograph of a coarse grained marble of the Marina Basement Unit with grain sizes up to 2–3 mm. Black arrow: triple junction of three calcite grains. White arrow: dynamically crystallized tabular Type IV twins (517971E, 4076999N). (d) Thin sections of garnet-biotite schists of the Marina Basement Unit: (i) Foliation wrapping around garnet porphyroblasts forming strain caps and strain shadows (XPL, 517609E, 4076249N). (ii) Cross-polarized light with tint plate photomicrographs showing a two-phase growth in a garnet with an inclusion-poor core and inclusion-rich rim. Biotite is growing in the strain shadows (516951E, 4074528N). (e) Ribbon endoskarms developed at the contact of the monzonite (mz) and white coarse-grained marbles (mb) (517123E, 4074259N). Subvertical banding shows alternating andradite garnet (adr) and hedenbergite (hd). (f) Wollastonite growing along a subvertical N-S striking joint plane, which crosscuts all earlier structures. Note that the length of individual crystals (example outlined by black arrows) exceeds a length of 30 cm (517211E, 4074309N).

4.4. Kos Detachment

The Kos Detachment is exposed across the whole Dikeos massif at the base of non-metamorphic limestone and dolostone klippen (Figure 7a). Although the exposed detachment planes dip in various directions making roughly an overall dome-shape, the stretching lineation uniformly trends NNW-SSE, with an overall top-to-SSE shear sense (black arrows, Figure 4d). Up to several meters below the detachment, rocks from the Dikeos Unit are phyllonitized and strongly overprinted by an SC and SCC' fabric recording top-to-SSE shear sense (Figure 7b). Qualitatively, the strain gradient, characterized by the intensity of phyllonitisation, increases in the footwall toward the detachment surface. In thin section, the phyllonites show evidence of brittle fracturing and ductile deformation by dissolution-precipitation creep (Figure 7c, where C' crosscut the S foliation in the clay-rich layer). Detachment folding, drag folding, SC and SCC' fabrics indicate top-to-SE directed shear deformation

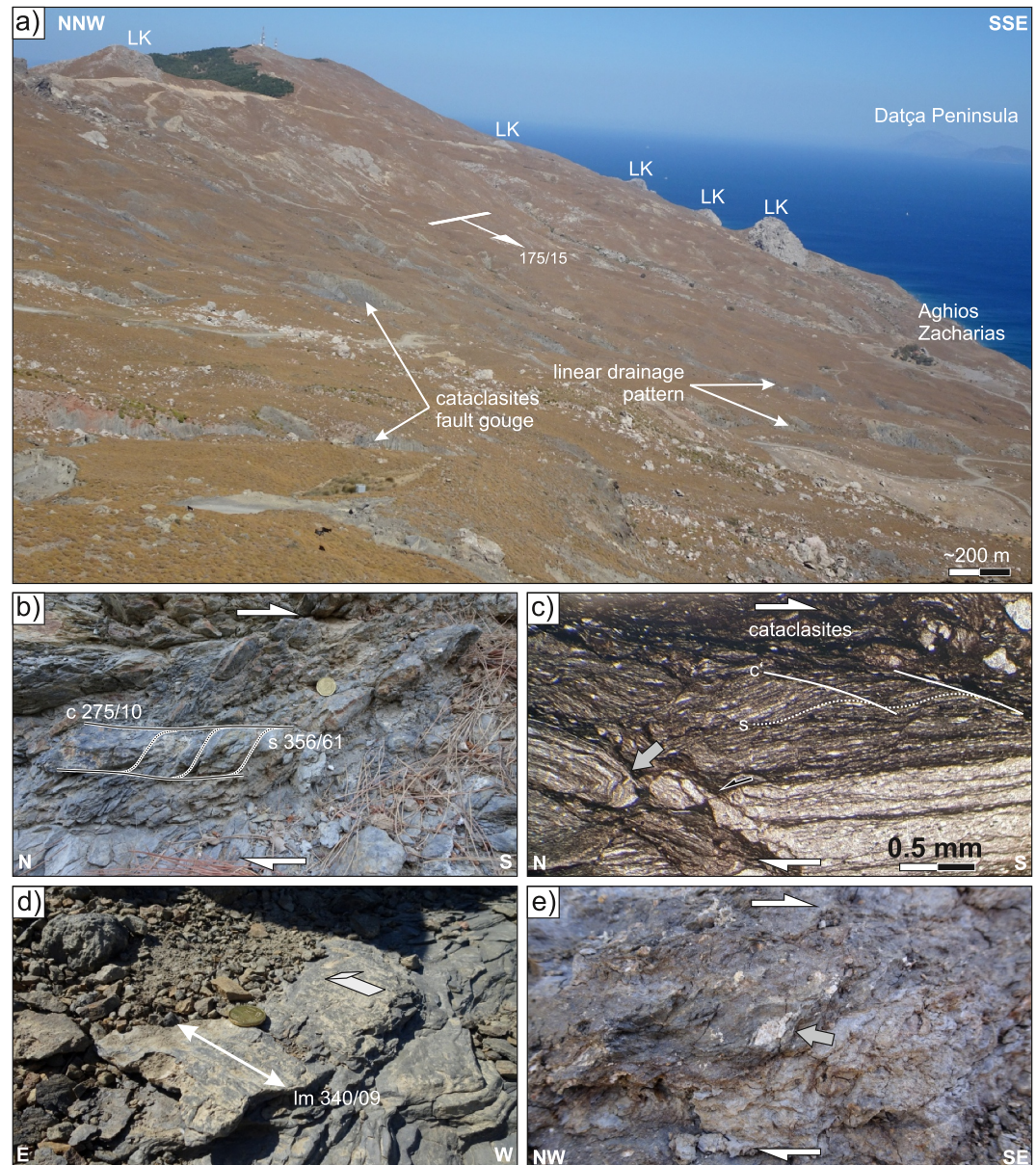


Figure 7. (a) View from Panagia Mamali (523572E, 4077615N) toward the east on the southern slope of the Dikeos massif. The Kos Detachment dips 15° parallel to the slope toward the south. The slope consists mainly of cohesionless cataclasites and fault gouges incised by a linear drainage pattern. Several unmetamorphosed limestone klippen (LK) of the Marina Cover Unit are preserved above the Kos Detachment. (b) Phyllonitized metaconglomerate in the Wildflysch Unit below the Kos Detachment (525614E, 4079623N). Sigmoidal-shaped, up to 10 cm diameter pebbles deformed in an SC-fabric record top-to-S shear sense of the Kos Detachment. (c) Thin section (PPL) photomicrograph of a graphitic phyllonite below the Kos Detachment close to Therma Beach (528475E, 4077774N) showing evidence for fracturing/cataclastic deformation and ductile folding (gray arrow), SC and SCC' fabrics formation by dissolution-precipitation creep. Black half arrow marks antithetic slip of a fractured quartz-rich layer. (d) Clay gouge at the base of a limestone klippe records a clear NNW-SSE trending stretching lineation (522702E, 4078271N). (e) Clay gouge below limestone klippe (522198E, 4078050N) shows crushed white dolomite sigmoids (gray arrow) and SC fabrics consistent with top-to-S shear sense.

(Figure 7c). The detachment surface is marked by a few meters thick fault clay gouge with a clear NNW-SSE trending striation (Figure 7d). Kinematic indicators in the fault gouge, such as SC and SCC' fabric in the clays, crushed sigmoidal objects of dolomite, and winged inclusions are consistent with the SSE-directed shear sense (Figure 7e). Although the fault rocks can be found at the base of each limestone klippe, the detachment plane is best exposed on the southern slope of the Dikeos massif above Embros Therma (Figure 3b, 4077672N,

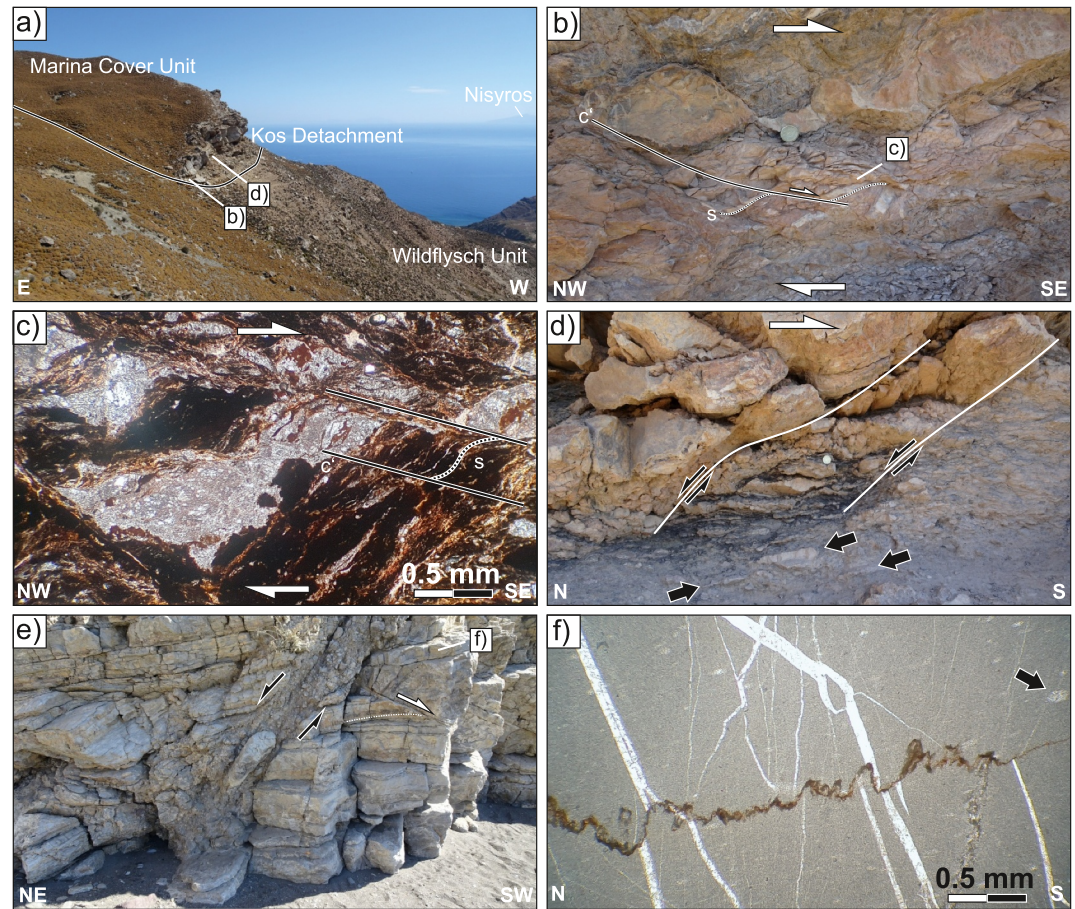


Figure 8. (a) Kos Detachment below a limestone klippe (Marina Cover Unit) and above the Wildflysch Unit. The picture is taken from location 523006E, 4077734N looking south. The internally undeformed limestones, which are dissected by some high-angle faults, rest on a zone of cataclastic deformation. The locations of panels (b) and (d) are noted. (b) Cataclastically deformed limestones with scaly fabrics overprinted by SCC' fabrics. Note that the C' planes continue in brittle high-angle faults in the hanging wall limestones, but the high-angle faults do not cut the fault rocks of the detachment. The location (523061E, 4077542N) of the sample for the thin section shown in (c) is noted. (c) Thin section (PPL) photomicrograph of a limestone cataclasite deformed by several cm-thick dissolution seams overprinted by a SCC' fabric. The shear sense is consistently top-to-S in accord with the kinematics of the Kos Detachment. (d) Antithetic high-angle faults in the limestone klippe above the fault rocks of the Kos Detachment, which have been rotated toward the south. Note that the faults root into the clay gouge/cataclasites and do not cross. Black arrows mark the preferred orientation of elongated limestone clasts in the fault gouge, consistent with the top-to-S shear of the Kos Detachment. (e) Localized top-to-S shear band (white half-arrow) deflects the bedding in chert-rich limestones. The shear band is cut by a brittle antithetic high-angle fault (528303E, 4077709N). The location of the sample shown in panel (f) is noted. (f) Thin section (PPL) photomicrograph of a micritic limestone, which shows no evidence of dynamic recrystallization. Dissolution-precipitation processes are documented by stylolites and perpendicular dissolved calcite veins. Black arrow marks a spheroidal unidentified relic of a fossil.

528206E). There erosion forms a dense linear drainage pattern in the highly erodible fault rocks with an average spacing between the channels of ~150–200 m (Figure 8a). For a detailed map of more than 50 klippen, see Triantaphyllis and Mavrides (1998). The base of the unmetamorphosed limestone klippen, which form the hanging wall of the Kos Detachment, is marked by a cataclastic shear deformation of the limestones overprinted by dissolution-precipitation deformation forming SCC' fabric (Figures 8a–8c). Movement along the Kos Detachment is also associated with the formation of high-angle faults in the limestones of the hanging wall. Although these high-angle faults formed as a conjugate set, most of the faults dip toward the north because of co-rotation of the bookshelf-type limestone blocks linked with antithetic slip along the high-angle faults. Here, the high-angle faults in the limestones do not crosscut the Kos Detachment but transfer their displacement into the detachment plane (Figure 8d).

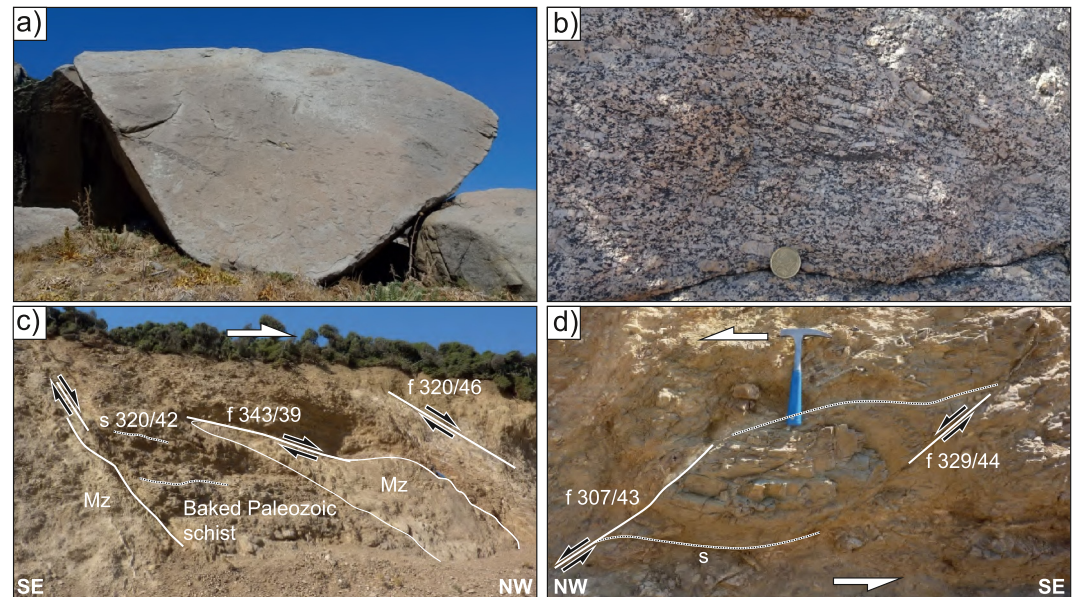


Figure 9. Photos of the monzonite intrusion. (a) Dam-scale block of monzonite in the Hippocrates boulder area northeast of Kardamena (515284E, 4074597N). The block is full of dioritic enclaves and enclave swarms, which preserve a magmatic flow fabric. (b) The magmatic flow fabric is also shown by preferred orientation of elongated orthoclase crystals (515294E, 4074591N). (c) Brittle deformation overprinting the monzonite (Mz) intrusion (514826E, 4075555N). Fault surface shows a clear N-S trending striation. (d) NW dipping cataclastic faults indicating a top-to-NNW sense of shear (514826E, 4075555N).

4.5. Marina Cover Unit

The rocks above the Kos Detachment are unmetamorphosed dolostones, dolomitic limestones, and micritic limestones with thick chert layers. The stratigraphic succession and thickness of this unit are unclear because it is only preserved as isolated klippen juxtaposed onto the metasediments of the Dikeos Unit along the Kos Detachment (Figure 7a). Surrounding the Dikeos massif, the carbonates are buried below Upper Miocene to Pleistocene sedimentary rocks and volcanic tuffs, with small exposures to the north and east. The limestones and dolostones are generally undeformed and sedimentary structures and bedding are well preserved. Only in the lower sections, some isolated, very localized m-scale shear bands, which are cut by brittle high-angle faults, reflect the S-directed shearing of the Kos Detachment (Figure 8e). In thin sections, the micritic limestones show no evidence of dynamic recrystallization of calcite. Yet, the limestones are strongly affected by dissolution-precipitation processes, as exhibited by intense stylolite formation with perpendicular dissolved calcite veins (Figure 8f). South of Pyli (Figure 3b, 4076082N, 515518E) and south of Zia (Figure 3b, 4076999N, 517971E), the partly dolomitized limestones locally pass into Eocene nummulitic limestones overlain by sandy flysch sediments representing the youngest stratigraphic section of the Marina Cover Unit on Kos (see also Triantaphyllis and Mavrides, 1998).

4.6. Miocene Monzonite Pluton

The western part of the Dikeos massif is intruded by a quartz-bearing biotite-hornblende monzonite with a surface diameter of ~4 km. Altherr et al. (1976) originally described the monzonite and provided detailed geochemical descriptions. Most of the intrusion does not record solid-state deformation, but locally cm-scale orthoclase crystals or swarms of elongated dioritic enclaves document a magmatic flow fabric (Figures 9a and 9b). A single tectonic contact between the limestones from the Marina Cover Unit, which only preserves a narrow contact metamorphism aureole close to the intrusion, and the monzonite could not be confirmed (cf. Altherr et al., 1976; van Hinsbergen and Boekhout, 2009). Conversely, our field observations suggest that this contact of the Marina Cover Unit to the monzonite is strongly overprinted by high-angle normal faults, most of which record a top-to-N offset. These roughly W-E striking high-angle normal faults are exposed on the western side of the island (Figure 3b). Locally, the top-to-N high-angle faults are associated with conjugate high-angle normal faults, which

Table 1
RSCM T_{max} Results

Sample	Location (UTM)		Total number of spectra	Mean R2	T_{max}	SD
	N	E				
K1	4077772	528483	17	0.6151	299	14
K2	4076993	517957	17	0.1709	565	35
K3	4076223	517662	17	0.1718	565	34
K4	4078506	520012	6	0.2932	510	98

Note. Indicated are the total number of Raman spectra performed on the sample, the mean R2 ratio, the RSCM temperature, and the uncertainty related to the intrasample heterogeneity. See location of the samples and results in Figures 3 and 4.

display a top-to-S offset, probably indicating brittle N-S extension (Figure 4e). Finally, the upper structural levels of the granitoid possess SC and SCC' fabric along north-dipping high-angle normal faults recording a top-to-N shear sense (Figures 9c and 9d).

5. Thermometry

Raman Spectroscopy of Carbonaceous Material (RSCM) analyses were conducted on four carbonaceous material-rich rocks (K1-K4) to determine the peak temperatures recorded by the different units (Figure 3, Table 1). Analyses were conducted following the laboratory protocol of Beyssac et al. (2002) at the ENS, Paris, France; details of the method, acquisition and processing are given in Supporting Information S1. Sample K1 is a graphitic phyllonite located in the upper part of the Dikeos Unit (i.e., Wildflysch Unit) below the Kos Detachment close to Therma Beach (Figure 3b). Samples K2

and K3 are from the Marina Basement Unit and consist of a coarse grained pure marble and a garnet schist, respectively. Sample K4 is a cataclasite with top-to-SSE fabrics from the Dikeos Unit located at the base of a limestone klippe below the Kos Detachment. Graphite is present in various clasts and in the ultrafine grained matrix.

RSCM results are projected onto a profile section (Figures 4a and 4b) and indicate a major temperature disparity between the Dikeos Unit and the Marina Basement. Indeed, the T_{max} of K1 is $299 \pm 14^\circ\text{C}$ whereas T_{max} of rocks from the Marina Basement is $565 \pm 35^\circ\text{C}$ (Table 1), suggesting a temperature difference of $>250^\circ\text{C}$. This is consistent with field observations indicating (a) a higher metamorphic grade (garnet-biotite schists) for rocks from the Marina Basement than rocks from the Dikeos Unit, and (b) no evidence for high grade metamorphic indices and ductile high strain deformation in the Dikeos Unit. Interestingly, K4 yields a large range of intra-sample temperatures from 360°C to 597°C that differs from other samples, implying a mixture of carbonaceous material (see the dispersion of the data in each sample, Table 1). Several factors can affect Raman-derived maximum temperatures in fault zones, including interaction with hot fluids, frictional heating, strain and inherited components (e.g., Kedar et al., 2020; Muirhead et al., 2021). Our interpretation for this T_{max} (i.e., burial depths) is equivocal because of the possibility of these complexities, and we therefore cannot estimate a mean temperature for this sample.

6. Geochronology

6.1. White Mica $^{40}\text{Ar}/^{39}\text{Ar}$ Geochronology

Multigrain, single crystal total fusion $^{40}\text{Ar}/^{39}\text{Ar}$ geochronology on handpicked, 106–250 μm mica separates from the Dikeos Unit was performed with a Photon Machines CO_2 laser coupled to an ARGUS VI mass spectrometer at the University of Manitoba, Winnipeg, Canada. The methodology and data tables (Table S1) are available in Supporting Information S1.

We dated 7–9 single, white mica crystals from five greenschist facies flyschoids that lie in the lowest grade isograds of Kalt et al. (1998) and one upper greenschist facies flysch from the western edge of the massif, <1 km from the intrusive contact with the monzonite. The detrital white micas form 0.25–1 mm large isolated grains, which are frequently squeezed, broken or kinked between neighboring other detrital quartz or feldspar grains (Figure 5c). The 50 single crystal dates range from c. 250 Ma to c. 450 Ma, with a dominant c. 300–330 Ma age population (Figure 10a). Even the dates from the sample closest to the Miocene intrusion, arguably within the contact aureole defined by Kalt et al. (1998), are not demonstrably different than the other more distal samples. Therefore, dates yield a robust Variscan age signature for the Dikeos Unit (Figure 10a).

6.2. Zircon (U-Th)/He Geochronology

Following standard mineral separation procedures, individual zircon grains from four samples of the Dikeos Unit in the eastern massif and one sample of Miocene monzonite were handpicked for (U-Th)/He dating. Five zircons from each sample were analyzed at the Thermochronology Research and Instrumentation Laboratory (U-Th)/He facility at the University of Colorado, Boulder, USA. Helium analyses were conducted using an ASI Alphachron

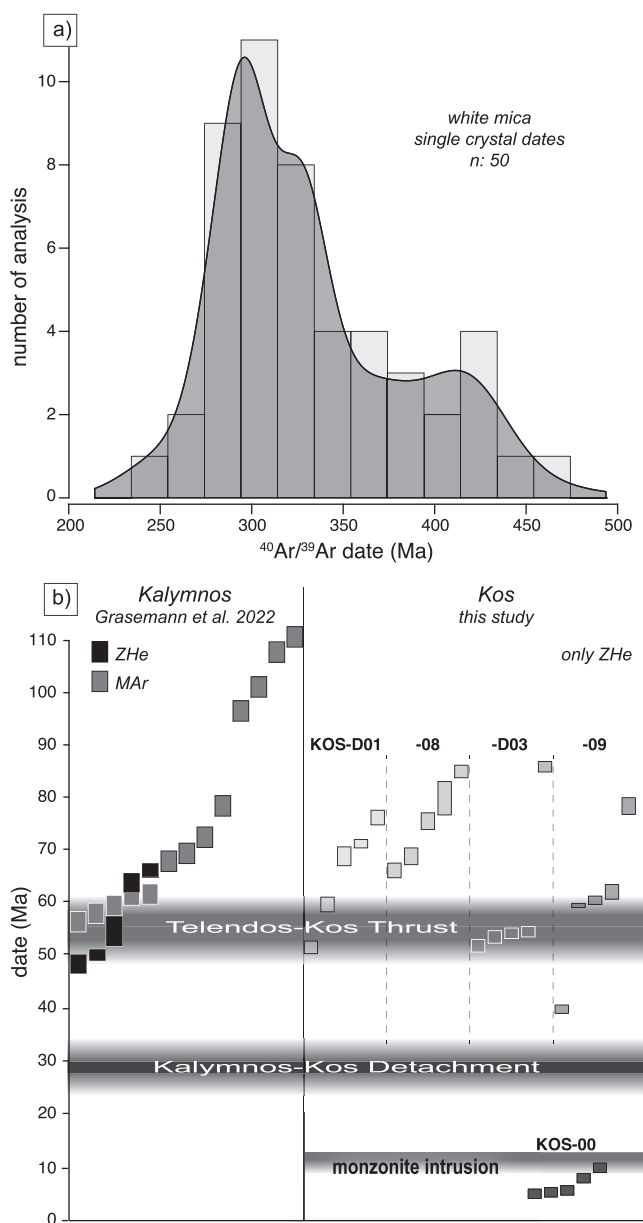


Figure 10. (a) Kernel density estimate plot and histogram of single crystal white mica $^{40}\text{Ar}/^{39}\text{Ar}$ dates ($n: 50$) from this study (kernel bandwidth: 15; histogram bin width: 20). Note the dominant Variscan age signature in the data. (b) Single zircon (U-Th)/He (ZHe) dates from four Wildflysch samples (Kos-D01, -D03, -08, -09) and one monzonite sample (Kos-00) from Kos. Each vertical bar is a single zircon date (2σ). Also plotted are single crystal ZHe and single crystal white mica $^{40}\text{Ar}/^{39}\text{Ar}$ dates from Kalymnos (Grasemann et al., 2022a). The timing of the Kalymnos Detachment is constrained by a population of (c) 30 Ma weighted mean ZHe ages (not plotted here; Grasemann et al., 2022a).

He extraction line connected to a Balzers PrismaPlus QME 220 quadrupole mass spectrometer. A Thermo Element 2 magnetic sector mass spectrometer was used for the U and Th analyses, and all ages were corrected for the effects of α ejection (Table S2). Details of the (U-Th)/He methodology are available in Supporting Information S1.

The new zircon (U-Th)/He (ZHe) data from the low grade metaflysch in the footwall of the Kos Detachment yield quite scattered single crystal dates that possess >20 Myr intrasample dispersion (Figure 10b). The oldest dates are Late Cretaceous, whereas the younger population is defined by earliest Eocene dates, and the ZHe dates have no clear relationship with effective uranium (eU) concentrations. The eU values, which are relatively high, can be used as a proxy for radiation damage of the zircon, where the lowest values signify arguably the most retentive crystals and should possess the oldest dates. Yet, the four lowest eU analyses (113–145 ppm) from three samples yielded dates between 51 Ma and 85 Ma, which essentially captures the entire range of dates dispersion within the whole data set. One sample, D03, was the most reproducible, with a weighted mean age of 53.5 ± 2.1 Ma (MSWD: 0.33; $n: 4$). The first-order impression of all of the ZHe data suggests the Dikeos Unit was below $\sim 200^\circ\text{C}$ since the earliest Eocene.

The 9–12 Ma monzonite intrusion exposed south of Pyli was sampled for ZHe geochronology. The analyses yielded single crystal dates from 10.3 to 4.8 Ma (Figure 10b), which possess extremely high eU values approaching 2,000 ppm. The ZHe dates are broadly consistent with existing biotite K-Ar dates and titanite fission track ages (Altherr et al., 1982) indicating a moderately slow cooling rate of the granitoid during the latest Miocene. Note that plutons in Cyclades, especially small ones, cool down relatively fast (e.g., Iglseider et al., 2009).

7. Discussion

7.1. Monzonite Kos Intrusion, Contact Metamorphism and Deformation

The Kos monzonite emplaced into the Dikeos Unit, pierced the Kos Thrust and the Kos Detachment (see triple point to the left of sample K3, Figure 3b), and intruded into the Marina Basement Unit producing a local contact metamorphic overprint and skarn assemblages. The pluton intruded at a depth of about 12 km at around 9–12 Ma (Altherr et al., 1976, 1982; Henjes-Kunst et al., 1988; Kalt et al., 1998) followed by a moderately slow cooling, which is supported by our ZHe dates of <10 Ma. Based on mineral paragenesis and experimentally derived phase relations, Altherr et al. (1976) suggested a host rock temperature of $\sim 800^\circ\text{C}$ at the contact of the pluton, which decreases to $\sim 500^\circ\text{C}$ over a distance of 4 km. Kalt et al. (1998) furthermore suggested that the contact metamorphism significantly overprinted non-metamorphic Paleozoic host rocks up to a distance of several kilometers; their biotite + muscovite-in and andalusite-in mineral isograds are at a distance of 4–5 km to the mapped contact of the intrusion. Thermometric calculations yielded surprisingly precise numbers of 762°C at 46 m from the monzonite contact, which decreases to 508°C at a distance of 1,258 m (Kalt et al., 1998).

Our field data and microstructural investigations, specifically the identification of inter-tectonic garnet, demonstrate that the monzonite intruded into a hitherto unrecognized garnet-bearing, ductily deformed Variscan metamorphic basement (i.e., Marina Basement Unit) as well as the Dikeos Unit and only support a very local contact metamorphic effect less than a few hundred of meters from the contact. Our new Variscan muscovite $^{40}\text{Ar}/^{39}\text{Ar}$ dates located at <1 km from the Miocene monzonite contact suggest that host rocks were not significantly affected by the metamorphic aureole, which is consistent with our field observations. In

addition, as the crystalline massif is within the largest Quaternary volcanic field in the Aegean (Smith et al., 1996), the preservation of a robust Variscan age signature is remarkable. A simple, one-dimensional first-order model describing the heating of rocks proximal to an instantaneously emplaced pluton is given by the thermal equilibration of a step-shaped temperature profile (e.g., Stüwe, 2007, eq. 3.88). Assuming 800°C for the temperature of the intrusion, 300°C for the ambient temperature of the host rocks (Altherr et al., 1976; our data), a thermal diffusivity of $10^{-6} \text{ m}^2 \text{ s}^{-1}$ and an intrusion diameter of 4 km (Triantaphyllis and Mavrides, 1998), results of the models indicate brief heating of the host rocks to temperatures above 500°C only to a distance of <600 m from the contact. This is in accord with our field observations that skarn mineralization occurs only a few hundred meters from the contact. Since all of the samples of Kalt et al. (1998) are apparently from the newly identified Marina Basement Unit, we speculate that except for local skarn minerals, the index minerals reported by Kalt et al. (1998) can be attributed to Variscan metamorphism and deformation. Notably, the scale of the metamorphic aureole is similar in size to metamorphic aureoles of other Miocene granitoids in the Cyclades (e.g., Lavrion, Tinos, Naxos, Marinos and Petrascheck, 1956; Jansen, 1977; Melidonis, 1980).

The absence of contact metamorphism in the Mesozoic to Paleogene klippen in the vicinity of the monzonite was already noticed by previous studies and has been interpreted as either top-to-S post-intrusion thrusting (Altherr et al., 1976; Papanikolaou and Nomikou, 1998) or top-to-N post-intrusion detachment faulting (van Hinsbergen and Boekhout, 2009). Our results show that the contact between the Marina Cover Unit and the monzonite is mostly faulted, and several W-E striking high-angle normal faults juxtaposed these units. In addition, the upper part of the Kos monzonite is overprinted by NW-dipping cataclastic faults (Figures 9c and 9d), suggesting that the N-S extension continued after pluton crystallization. These numerous low-angle faults may have been rotated toward the south at lower angles recording antithetic top-N slip or may suggest the presence of a brittle top-to-N detachment above the intrusion, which has been locally eroded. Similar observations have been reported by van Hinsbergen and Boekhout (2009), which led them to propose the existence of a top-to-N detachment on Kos (Figure 6 of van Hinsbergen and Boekhout, 2009). The solution of fault rotation seems more likely, because all the units in the region are reworked by high-angle normal faults that control graben formation during this period. The current morphology of the island has been tilted toward the north by a Quaternary fault zone along its southern coast.

7.2. Kinematics and Age of the Kos Detachment and Kos Thrust

The onset of crustal extension and the timing of faulting are more difficult to determine since the Kos Detachment is localized in the brittle crust forming clay gouges and cataclases. The fault rocks of the Kos Detachment can be observed at the base of all limestone klippen (i.e., Marina Cover Unit). Macroscopic and microscopic kinematic indicators unequivocally demonstrate that the Kos Detachment has top-to-S kinematics (Figure 7). The top-to-N high-angle faults in the hanging wall of the detachment can be easily explained by a bookshelf model that involves co-rotation of fault-bounded blocks recording antithetic shear between the blocks, especially if the displacement of the high-angle faults is transferred into the low-angle detachment (Figures 8d and 8e). The Kos Thrust has a comparable brittle signature causing few practical geochronometers to be appropriate for resolving the timing of deformation, so this crosscutting relationships can be useful as a first-order estimate. The monzonite pierces the Kos Detachment and crosscuts the Kos Thrust, suggesting that the Kos Thrust and the Kos Detachment operated before the late Miocene intrusion. Furthermore, the Kos Detachment crosscuts the Kos Thrust (see termination of the Kos Thrust north of sample K3, Figure 3b), indicating that displacement along the Kos Thrust was earlier than the activity of the Kos Detachment. ZHe data from the footwall of the top-to-N Kos Thrust indicate partial thermal resetting in the Paleocene, including a fully reset ZHe age for sample D03 at c. 54 Ma. Interestingly, 20 km to the north, a population of mica $^{40}\text{Ar}/^{39}\text{Ar}$ and ZHe dates from rocks below the Kalymnos Detachment, and proximal to the Telendos Thrust, similarly yield Paleocene ages. On Kalymnos, this has been interpreted to be related to top-to-N displacement along the Telendos Thrust during shortening of the Pelagonian domain in the upper plate above the subducting Pindos ocean (Grasemann et al., 2022a). We invoke an analogous scenario on Kos: faulting along the Kos Thrust is Paleocene in age. Furthermore, based on ZHe dates, the top-to-SSW Kalymnos Detachment, which was active under slightly warmer conditions than the Kos Detachment, has been suggested to exhume and cool the footwall at c. 30 Ma (Grasemann et al., 2022a). The Kalymnos Detachment is localized at the base of the Marina Cover Unit in Verrucano-type violet shales and yellow dolomites that occur below the Mesozoic limestones (Grasemann et al., 2022a). These Permo-Triassic Verrucano-type sediments have not been observed on Kos, where instead the base of the limestone klippen of the Marina Cover Unit is always marked by

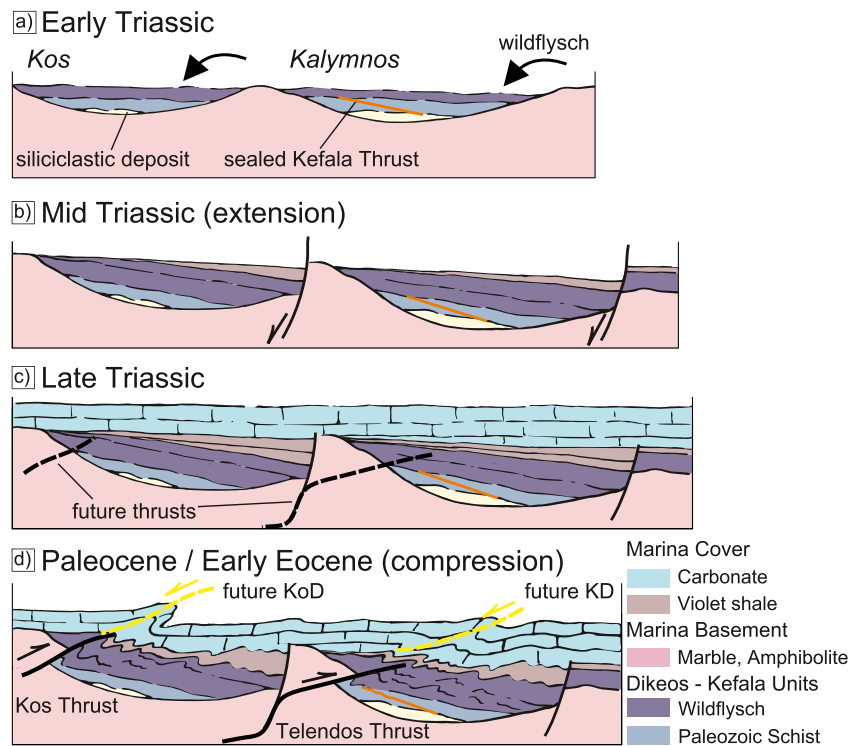


Figure 11. Schematic reconstruction of the geology in the Kos-Kalymnos region between the Late Permian and Paleocene—early Eocene modified from Grasemann et al. (2022a).

several meter-thick clay gouges and non-cohesive ultra-cataclasites, which are the fault rocks of the top-to-S Kos Detachment. Although we cannot rule out an earlier activity of the Kos Detachment, we prefer an analogy to the Kalymnos Detachment with Oligocene activity that is supported by the widespread deposition of mid-Upper Eocene flysch onto the hanging wall (i.e., Marina Cover Unit) in the central-north Dodecanese.

7.3. Regional Lithological Correlation

The Dikeos Unit experienced only a low grade metamorphic overprint as evinced by the lower greenschist facies mineral assemblages of the samples and T_{max} of sample K1, and there is no obvious tectonic contact between the Paleozoic and Wildflysch units as previously mapped (van Hinsbergen and Boekhout, 2009). The Dikeos Unit may correspond to the Phyllite Quartzite Unit, which is situated between the Ionian and Gavrovo-Tripolitza units on Crete (Bonneau, 1984; Creutzburg et al., 1977) and reached blueschist facies condition during the early Miocene (Jolivet et al., 1996), yet this is not the case for the Dikeos Unit. The absence of a wildflysch in the Phyllite Quartzite Unit combined with the absence of high-pressure paragenesis in the Dikeos Unit exclude a possible correlation between these units. Alternatively, it is conceivable to correlate the Dikeos Unit to the Kefala Unit on nearby Kalymnos, which is part of the structurally highest Pelagonian domain. This unit mainly includes imbricated and folded Upper Paleozoic fossil-rich limestones and marbles with siliciclastic intercalations unconformably overlain by a wildflysch that is most likely Early Triassic in age (Grasemann et al., 2022a; Kähler, 1987). Similar to Kalymnos, hectometer-scale blocks of marble and gabbroic rocks occur as olistoliths in sandstones and conglomerates of the Kos Wildflysch Unit. Additionally, in both wildflysch units, $^{40}\text{Ar}/^{39}\text{Ar}$ dates of detrital white mica that are partially reset on Kalymnos, but not on Kos, suggest detritus from a Variscan metamorphic hinterland (new data here and Grasemann et al., 2022a). The major difference of the wildflysch between the islands is that the wildflysch on Kalymnos records a transgressive contact with the underlying folded and faulted Upper Paleozoic limestones and marbles. Such an angular unconformity is not exposed on Kos, but instead the Wildflysch Unit shows a sedimentary transition into the underlying Paleozoic Unit. We therefore decided to correlate the Dikeos Unit to the Kefala Unit (Figure 11), implying local variations in the Paleozoic paleogeography of the Pelagonian domain.

The higher grade metamorphic Marina Basement Unit on Kos is juxtaposed on top of the lower grade Dikeos Unit along a ductile to brittle top-to-N thrust (Figure 11). Thrusting is supported by a strain gradient from ductile to brittle deformation in the hanging wall toward the thrust surface and by the RSCM temperature difference from 565°C to 299°C (Table 1). On Kalymnos, a similar structural position of the Marina Basement Unit, with a Variscan affinity, has been displaced to the north onto a presumably Triassic wildflysch along the ductile-to-brittle Paleocene Telendos Thrust (Grasemann et al., 2022a). We, therefore, suggest correlating these units, which are 20 km apart (Figure 11). The Marina Basement Unit on both Kalymnos and Kos possess quartzites and garnet-bearing quartz-mica schists and internally complex re-fold Type 2 and 3 structures. Lithological differences include the lack of amphibolites on Kos and the fact that no marbles have been reported from Kalymnos. Furthermore, the Marina Basement Unit on Kos is strongly overprinted by contact metamorphic skarns along the margins of the Miocene monzonite pluton, which pierced the Kos Thrust.

The Mesozoic carbonates in the Dodecanese have been correlated with the Lycian Nappes (Bernoulli et al., 1974; Dürr et al., 1978), with the Gavrovo-Tripolitza Unit (Jolivet et al., 2004; Papanikolaou and Demirtasli, 1987; Ring et al., 2010) or with the Pelagonian domain (Dürr et al., 1978; Mountrakis, 1986; Schmid et al., 2020). Based on an Early-Mid Cretaceous unconformity, which is common for the Pelagonian yet has not been reported from the Gavrovo-Tripolitza platform (e.g., Clift & Robertson, 1990; Scherreiks et al., 2014), and the tectonic position of the rocks on Kalymnos (including the Marina Cover Unit) above the Cycladic Blueschist Unit in the northern Dodecanese (Roche et al., 2018), Grasemann et al. (2022a, 2022b) recently suggested that the unmetamorphosed para-autochthonous limestones on Telendos, Kalymnos and Pserimos are part of the Pelagonian domain. On Kos, two types of non-metamorphic limestone klippen above the Kos Detachment have been described (Triantaphyllis and Mavrides, 1998): (a) Jurassic medium- to thin-bedded limestones with abundant chert nodules, and (b) Cretaceous white-gray, thick-bedded limestones. The Gavrovo-Tripolitza Unit does not possess Jurassic cherty limestones, which precludes a correlation with the Kos limestones. In contrast, these lithologies strongly resemble the Mesozoic limestone sequence of the Marina Cover Unit described from Telendos, Kalymnos, and Pserimos to the north (Figure 11; Dounas et al., 1983; Tselepidis and Carras, 2013; Grasemann et al., 2022a, 2022b).

The limestones on Kos are conformably overlain by mid-Upper Eocene flysch, which results in implications for regional correlations. First, the Eocene ages exclude similarities with metaflysch from the Datça Peninsula (Orombelli et al., 1967), the metaflysch of the Karabörtlen Formation described in the Bodrum area directly to the east (Bernoulli et al., 1974) and the Pindos flysch that starts in the latest Cretaceous-Paleocene and ends in the Eocene (Papanikolaou, 2021). Second, considering (a) the absence of a tectonic contact between the mid-Upper Eocene nummulitic flysch and the limestones on Kos, and (b) the limestones belong to the Marina Cover, a correlation of the flysch with the Basal Unit is excluded. Based on the observations from Pserimos (Christodoulou, 1970; Desio, 1931; Grasemann et al., 2022b), where the Pelagonian Mesozoic platform carbonates are also overlain by Eocene flysch, we suggest that the Marina Cover Unit on Kos including the Eocene flysch are part of the Pelagonian domain.

Combining these observations, we propose a simplified model, similar to the model of Grasemann et al. (2022a), of paleogeographic evolution for Kos and Kalymnos ranging from the Early Triassic to the Paleocene-Eocene (Figure 11). In the Early Triassic (Figure 11a), lithospheric scale shortening induced by the closure of the Paleotethyan Ocean lead to a cycle of uplift and erosion of the Pelagonian rocks, including the Dikeos Unit and the Kefala Unit, that could belong to the structurally highest Pelagonian domain. Deposition also occurred during this period, and deformation may have affected the limestones of the different units (e.g., Kefala Thrust on Kalymnos). In mid-Triassic (Figure 11b), the Paleotethyan accretionary prism and Pelagonian Variscan basement (e.g., Marina Basement Unit) were dissected by a localized rifting event. Similar to Kalymnos, the Marina Basement Unit and the Dikeos Unit reached the surface on Kos. Then, the tectonic activity decreased in the entire area due to the expansion of the oceanic domains (Vardar-Axios and Pindos), implying the deposition of a carbonate platform (Figure 11c). Finally, in the Paleocene-Eocene (Figure 11d), the subduction of the Cycladic Blueschist Unit toward the north below the Pelagonian created local back-thrusts in the upper plate. These top-to-N back-thrusts correspond to the Kos and Telendos thrusts. They brought the Marina Basement Unit above the Dikeos Unit and Kafala Unit.

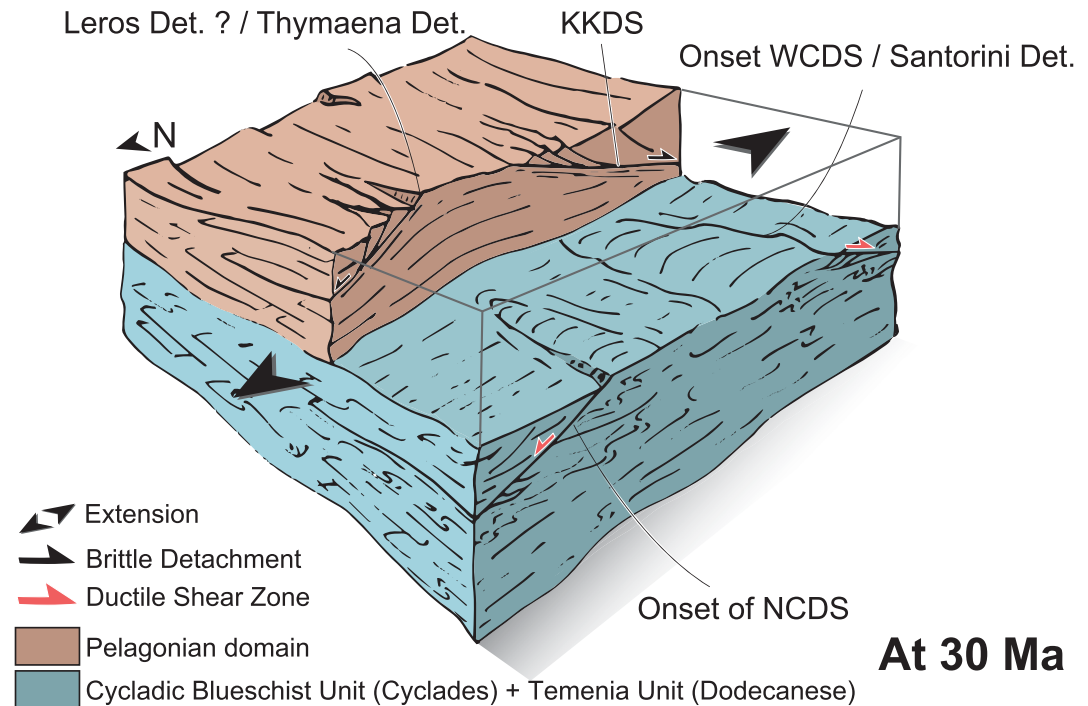


Figure 12. Simplified 3D diagram showing the localization of deformation across the Aegean region at c. 30 Ma. Note that the distance between the detachments and shear zones is not to scale.

7.4. Oligocene Extension in the Aegean Domain Versus Oligocene Compression in Western Turkey

Post-orogenic extension started ~ 20 Myr before the emplacement of the intrusion, by considering an age of 30 Ma for the Kos Detachment. After a period of convergence that formed an orogenic wedge, including the activity of the two thrusts in the Pelagonian domain during the Paleocene, post-orogenic extension commenced during the Oligocene in the Dodecanese. Initiation of extension corresponded to a drastic change in the subduction dynamics in which southward slab retreat started in the entire Aegean domain (Jolivet and Brun, 2010; Jolivet and Faccenna, 2000). Deformation in northern and central Dodecanese is mostly brittle, and extension is mainly accommodated by the top-to-S Kalymnos and Kos detachments, which were active under slightly different temperature conditions. Such a cooler condition of Kos Detachment implies that deformation is localized at higher structural levels compared to the Kalymnos Detachment. We propose to group these two structures into a crustal-scale system called the Kalymnos-Kos Detachment System (KKDS), which is notably localized within the Pelagonian domain (Figure 12). To the north, brittle deformation is also associated with detachment faults. Roche et al. (2019) reported a tectonic contact between the low metamorphic grade rocks of the Fourni Unit and the non-metamorphic, upper Mesozoic limestones of the Thymaena Unit on the Thymaena Islands that belong to the Pelagonian domain. The contact is marked by 20 m thick clay gouges and yellowish, foliated cataclasites with shear criteria indicating top-to-NNE deformation (Roche et al., 2019). Even though tectonic markers are opposite to the KKDS activity (i.e., top-to-NNE in Thymaena Islands), deformation is very similar (brittle) and localizes at the base of the Mesozoic unmetamorphosed limestones. On Leros, the Marina Cover of Mesozoic limestones and violet shales and the Marina Basement of amphibolites and mica schists are also present, but the contact between these sub-units was poorly studied (Roche et al., 2018). However, its kinematics can be estimated indirectly. If we consider that the Temenia Unit belongs to the most external part of the Cycladic Blueschist Unit (following Roche et al., 2018), then peak-burial conditions have been recorded during the Eocene. Roche et al. (2018) also revealed that the Temenia unit had been then exhumed under the Marina Unit through top-to-NE ductile to brittle shearing implying a continuum of deformation. Several conclusions may be made: (a) The brittle activity of the tectonic contact between the Marina Cover and the Marina Basement on Leros (i.e., the Leros Detachment) is probably top-to-NE; (b) this contact is localized in the Pelagonian domain at the base of the Marina Cover Unit in Verrucano-type violet shales similar to the Kalymnos Detachment (Grasemann et al., 2022a). To summarize, although there is a lack of geochronological constraints to interpret the tectonic activity along these detachments,

we propose that top-to-N detachments (Thymaena and Leros?) are synchronous with the KKDS, implying a crustal-scale bivergent extension pattern during the Oligocene (Figure 12; Grasemann et al., 2022a), which appears to be mainly restricted to the upper crust. Nonetheless, the major difference between the Dodecanese Islands is the presence of the Temenia Unit exposed on the islands of Leros, Lipsi and Arki (Roche et al., 2019). We speculate that extension is important in this region, exhuming the deeper rocks that recorded Alpine high-pressure metamorphism.

Contemporaneous with Oligocene extension observed in the Dodecanese area (Grasemann et al., 2022a; this study), a pervasive shearing also occurs at the base of the Pelagonian domain, affecting the lower unit—that is the Cycladic Blueschist Nappe—in the Cyclades (Figure 12, see above). Indeed, ductile deformation localizes at this time and is observed along the North Cycladic Detachment System (NCDS, Jolivet et al., 2010), West Cycladic Detachment System (WCDS, Grasemann et al., 2012) and Santorini Detachment (Schneider et al., 2018). The kinematics are not the same within the shear zones, in particular, the NCDS and the WCDS exhibit opposing sense of shear (top-to-NE and top-to-SW, respectively). At the regional scale, ductile and brittle crustal deformation appears fairly symmetrical. The “spreading” of the crust may be also favored by antiformal stacking of mid-crustal slices that triggers vertical tectonic uplift within the subduction zone (Platt, 1986). In that case, the upward movement of the Basal Unit could generate gravity-driven extension in the hanging wall of the contact between the Basal Unit and the Cycladic Blueschist Unit. Overall, the exhumation of the blueschist unit is facilitated by the brittle extension recorded in the Pelagonian domain (Figure 12).

Deformation is also recorded in southwestern Turkey, but the kinematics are debated in the literature. Collins and Robertson (2003) proposed that the Lycian nappes were thrust to the southeast upon the Menderes Massif and the Bey Daglari platform during the latest Cretaceous to late Miocene. The implication is that deformation in southwestern Turkey appears to record only compressional tectonics. Conversely, Rimmelé et al. (2003) suggested that the Lycian Nappes records two stages of exhumation: (i) the first one between the Late Cretaceous and the late Eocene characterized by a top-to-NE shearing and high-pressure metamorphism associated with syn-orogenic exhumation, whereas (ii) the second stage occurs in the Miocene synchronous with Aegean extension. The difference in these models can partly be explained by a lack of geochronological constraints. Post-orogenic extension in this region likely started before the Miocene as is the case in the central Dodecanese and Cyclades. Lips et al. (2001) have also reported that regional extension started during Eocene-Oligocene in the Menderes Massif, which is located below the Lycian Nappe. Overall, the connection between these different domains is essential for understanding the subduction dynamics during this period.

7.5. Miocene Intrusions and Extension

In the Aegean-Anatolian domain, plutons are mostly exposed in metamorphic core complexes and were exhumed by detachment faults recording a complete evolution from the magmatic flow fabric to localized deformation (e.g., Gaudreau et al., 2017; Isik et al., 2004; Jolivet et al., 2021; Rabillard et al., 2018). Geochemical data indicate that granites originated from variable sources, mainly metaigneous, are not related to the Hellenic subduction zone but rather associated with the back-arc extension (Altherr & Siebel, 2002). Such is not the case for the Kos monzonite, which shows the involvement of a mantle-derived component (Soder et al., 2016), similar to the Samos intrusion dated to c. 10 Ma (Mezger et al., 1985). The Kos intrusion was followed by numerous vertical, NNE-to-NNW striking lamprophyre dikes, which also have strong isotopic and chemical similarities to rocks that erupted along the South Aegean volcanic arc (Soder et al., 2016). Dikes of similar chemical composition and age from the Bodrum Volcanic Complex occur in the Bodrum peninsula (Robert et al., 1992). We propose that these mantle-derived melts underline the slab tearing which is documented beneath western Turkey by numerous mantle tomography studies (e.g., Berk Biryol et al., 2011; Bijwaard et al., 1998) and through magmatic evolution (e.g., Dilek & Altunkaynak, 2009). In particular, we speculate that the orientation of dikes on Kos is related to the large sinistral lithospheric shear zone activity (Gessner et al., 2013; Roche et al., 2019) that accommodates the difference rates of extension between western Turkey and the Aegean domain.

Further, our results identified cataclasites in the upper part of the monzonite. The absence of ductile deformation related to faulting differs from the other Miocene intrusions where a continuum of deformation from ductile to brittle within the granitoid is reported (Jolivet et al., 2021; Rabillard et al., 2018). Here, the intrusion provides a rheological contrast with the host rocks, which favors the localization of deformation after its emplacement in the upper part of the crust. For example, such an observation has been described on the pluton of Mykonos Island

(Rabillard et al., 2018). After cooling, the strength contrast between the pluton and the Pelagonian rocks, on the one hand, and the sediments of the Neogene basin on the other hand, allows the deformation to be localized. Extensional deformation then results in the formation of a low-angle brittle normal fault, the Mykonos detachment, which is localized at the interface between the metamorphic core complex and overlying sediments. This lack of continuum of deformation from ductile to brittle in the Kos monzonite seems to exclude the presence of a detachment and therefore confirms that the low-angle faults were rotated toward south at lower angles. Overall, the N-S extension in the central Dodecanese prevailed after the intrusion of the monzonite on Kos, as suggested by W-E striking high-angle faults cutting the pluton, and is still active, indicated by the WNW-ESE striking horst-graben morphology on Kalymnos and damaged speleothems on Pserimos (Grasemann et al., 2022a, 2022b). This implies that Neogene extension related to slab retreat and tearing maintained a constant N-S extension at the crustal scale.

8. Conclusion

1. We proposed a new tectonostratigraphy of the Paleozoic to Neogene rocks on Kos including:
 - a depositional contact between the Paleozoic Unit and the Permo-Triassic Wildflysch Unit;
 - the Marina Unit that was thrustured during the Paleocene onto the low grade Paleozoic Unit and Wildflysch Unit with top-to-N kinematics;
 - the Oligocene Kos Detachment that is localized below the unmetamorphosed Mesozoic limestones showing top-to-S kinematics;
 - the monzonite pluton and its narrow (a few hundred meters) metamorphic aureole, which crystallized between 9 and 12 Ma and recorded a moderately slow cooling.
2. At the regional scale, we suggested that:
 - The Pelagonian domain can be extended to the northern part of the central Dodecanese. It includes the Dikeos Unit, which corresponds to the structurally lower Pelagonian rocks, the higher grade metamorphic Marina Basement Unit, the Mesozoic-Eocene Marina Cover and the mid-Upper Eocene flysch.
 - In the central Dodecanese Islands, the Oligocene extension was bivergent and accommodated along the top-to-S KKDS in the south, and along a series of top-to-N detachments in the north, mainly localized in the Pelagonian upper plate.
 - In the Cyclades, and a few Myr later, the deformation started to propagate to deeper structural levels within the base of the Pelagonian, affecting the rocks of the Cycladic Blueschist Unit and favoring their fast exhumation. In western Turkey, a lack of consensus on deformation pattern limits a broader understanding of this process, but the connection between the Dodecanese and Cyclades is essential to constrain the subduction dynamics.
 - The Kos intrusion is similar to the Samos intrusion, and differs from metamorphic core complex-related intrusions. The mantle component of the magma and the orientation of lamprophyre dikes are interpreted as surface indicators of the slab tearing at depth occurring beneath western Turkey.
 - After the emplacement of the Kos intrusion, N-S extension continued in the entire central Dodecanese, controlling the current geomorphology of islands. Deformation pattern related to slab retreat and tearing is therefore N-S, limiting the strike-slip component that is expected above a tear.

Data Availability Statement

The data is available in Supporting Information S1, tables, and figures for the purposes of peer review. Raman spectra were analyzed with Peakfit software (v4.06) available in platform at the following link <https://grafiti.com/fr/peakfit/>.

References

- Allen, S. R., Stadlbauer, E., & Keller, J. (1999). Stratigraphy of the Kos Plateau Tuff; product of a major Quaternary explosive rhyolitic eruption in the eastern Aegean. *Greece Journal of Earth Sciences*, 88(1), 132–156. <https://doi.org/10.1007/s005310050251>
- Altherr, R., Keller, J., & Kott, K. (1976). Der jungtertiäre Monzonit von Kos und sein Kontaktof (Agäis, Griechenland). *Bulletin de la Societe Geologique de France*, 7, 403–412.
- Altherr, R., Kreuzer, H., Wendt, I., Lenz, H., Wagner, G. A., Keller, J., et al. (1982). A late Oligocene/early Miocene high temperature belt in the Attic-Cycladic crystalline complex (SE Pelagonian, Greece). *Geologisches Jahrbuch*, E23, 97–164.
- Altherr, R., & Siebel, W. (2002). I-type plutonism in a continental back-arc setting: Miocene granitoids and monzonites from the central Aegean Sea, Greece. *Contributions to Mineralogy and Petrology*, 143(4), 397–415. <https://doi.org/10.1007/s00410-002-0352-y>
- Bachmann, O., Allen, S. R., & de Maisonville, C. B. (2019). The Kos–Nisyros–Yali volcanic field. *Elements*, 15(3), 191–196. <https://doi.org/10.2138/gselements.15.3.191>

Acknowledgments

Funding was provided by the Austrian Academy of Sciences (Grant FA536037) (Emil Suess-Erbschaft) and by the Natural Sciences and Engineering Research Council of Canada. We thank the Hellenic Survey of Geology and Mining Exploration (HSGME) in Athens for technical support and providing permission for fieldwork. Laboratory assistance from Jim Metcalf (University of Colorado) and Alfredo Camacho (University of Manitoba) is greatly appreciated. We thank the two anonymous reviewers and the associate editor, Federico Rossetti, for their constructive comments, which improved the paper.

- Berk Biryol, C., Beck, S. L., Zandt, G., & Özacar, A. A. (2011). Segmented African lithosphere beneath the Anatolian region inferred from teleseismic P-wave tomography. *Geophysical Journal International*, *184*(3), 1037–1057. <https://doi.org/10.1111/j.1365-246X.2010.04910.x>
- Bernoulli, D., Graciansky, P. C., & Monod, O. (1974). The extension of the Lycian Nappes (SW Turkey) into the southeastern Aegean Islands. *Eclogae Geologicae Helveticae*, *67*, 39–90.
- Beysac, O., Goffé, B., Chopin, C., & Rouzaud, J. N. (2002). Raman spectra of carbonaceous material in metasediments: A new geothermometer. *Journal of Metamorphic Geology*, *20*(9), 859–871. <https://doi.org/10.1046/j.1525-1314.2002.00408.x>
- Bijwaard, H., Spakman, W., & Engdahl, E. R. (1998). Closing the gap between regional and global travel time tomography. *Journal of Geophysical Research*, *103*(B12), 30055–30078. <https://doi.org/10.1029/98jb02467>
- Bonneau, M. (1984). Correlation of the Hellenide nappes in the south-east Aegean and their tectonic reconstruction. In J. E. Dixon & A. H. F. Robertson (Eds.), *The geological evolution of the eastern Mediterranean* (Vol. 17, (1), pp. 517–527). Geological Society, London, Special Publications. <https://doi.org/10.1144/gsl.sp.1984.017.01.38>
- Bozkurt, E., Satir, M., & Buğdaycıoğlu, Ç. (2011). Surprisingly young Rb/Sr ages from the Simav extensional detachment fault zone, northern Menderes Massif, Turkey. *Journal of Geodynamics*, *52*(5), 406–431. <https://doi.org/10.1016/j.jog.2011.06.002>
- Bröcker, M., Baldwin, S., & Arkudas, R. (2013). The geological significance of $^{40}\text{Ar}/^{39}\text{Ar}$ and Rb–Sr white mica ages from Syros and Sifnos, Greece: A record of continuous (re) crystallization during exhumation? *Journal of Metamorphic Geology*, *31*(6), 629–646. <https://doi.org/10.1111/jmg.12037>
- Brun, J.-P., & Faccenna, C. (2008). Exhumation of high-pressure rocks driven by slab rollback. *Earth and Planetary Science Letters*, *272*(1–2), 1–7. <https://doi.org/10.1016/j.epsl.2008.02.038>
- Christodoulou, G. (1970). Some remarks on the geology of Kalymnos island (Dodecanes) and the age of its formations. *Annales Geologique de Pays Hellenique*, *21*, 307–319.
- Clift, P. D., & Robertson, A. H. F. (1990). A Cretaceous Neo-Tethyan carbonate margin in Argolis, southern Greece. *Geological Magazine*, *127*(4), 299–308. <https://doi.org/10.1017/s0016756800014862>
- Coleman, M., Schneider, D. A., Grasemann, B., Soukis, K., Lozios, S., & Hollinetz, M. S. (2020). Lateral termination of a Cycladic-style detachment system (Hymittos, Greece). *Tectonics*, *39*(9), 1–9.30. <https://doi.org/10.1029/2020tc006128>
- Collins, A. S., & Robertson, A. H. (1997). Lycian melange, southwestern Turkey: An emplaced Late Cretaceous accretionary complex. *Geology*, *25*(3), 255–258. [https://doi.org/10.1130/0091-7613\(1997\)025<0255:LMSTAE>2.3.CO;2](https://doi.org/10.1130/0091-7613(1997)025<0255:LMSTAE>2.3.CO;2)
- Collins, A. S., & Robertson, A. H. (2003). Kinematic evidence for Late Mesozoic–Miocene emplacement of the Lycian allochthon over the western Anatolide belt, SW Turkey. *Geological Journal*, *38*(3–4), 295–310. <https://doi.org/10.1002/gj.957>
- Creutzburg et al., 1977 Creutzburg, N., Drooger, C. W., Meulenkamp, J. W., Papastamatiou, J., Seidel, E., & Tataris, A. (1977). General Geological Map of Crete. Institute of Geological and Mining Exploration (IGME), scale 1:200,000.
- De Boorder, H., Spakman, W., White, S. H., & Wortel, M. J. R. (1998). Late Cenozoic mineralization, orogenic collapse and slab detachment in the European Alpine Belt. *Earth and Planetary Science Letters*, *164*(3–4), 569–575. [https://doi.org/10.1016/S0012-821X\(98\)00247-7](https://doi.org/10.1016/S0012-821X(98)00247-7)
- Desio, A. (1931). Le isole italiane d'Il'legeo, Roma. Memorie descrittive della carta geologic' d'Italia (p. 534).
- Dilek, Y., & Altunkaynak, Ş. (2009). Geochemical and temporal evolution of Cenozoic magmatism in western Turkey: Mantle response to collision, slab break-off, and lithospheric tearing in an orogenic belt. *Geological Society London, Special Publications*, *311*(1), 213–233. <https://doi.org/10.1144/SP311.8>
- Dounas et al., 1983 Dounas, A. G., Kakavas, N. J., & Tassios, N. P. (1983). Geological map of Greece, sheet Kalymnos island. IGMA, scale 1:50000.
- Ducharme, T., Schneider, D. A., Grasemann, B., & Klonowska, I. (2022). Exhumation by combined coaxial and non-coaxial strain along the Evia Shear Zone (southern Evia, Greece). *Tectonics*, *41*(12), 1–28. <https://doi.org/10.1029/2022tc007561>
- Dürr, S., Altherr, R., Keller, J., Okrusch, M., & Seidel, E. (1978). The median Aegean crystalline belt: Stratigraphy, structure, metamorphism, magmatism. In H. Cloos, D. Roeder, & K. Schmidt (Eds.), *Alps, Apennines, Hellenides* (Vol. 38, pp. 455–476). Stuttgart.
- Fassoulas, C., Kilias, A., & Mountrakis, D. (1994). Postnappe stacking extension and exhumation of high-pressure/low-temperature rocks in the island of Crete, Greece. *Tectonics*, *13*(1), 127–138. <https://doi.org/10.1029/93TC01955>
- Ferrill, D. A., Morris, A. P., Evans, M. A., Burkhard, M., Groshong, J., Richard, H., & Onasch, C. M. (2004). Calcite twin morphology: A low-temperature deformation geothermometer. *Journal of Structural Geology*, *26*(8), 1521–1529. <https://doi.org/10.1016/j.jsg.2003.11.028>
- Franz, L., Okrusch, M., Seidel, E., & Kreuzer, H. (2005). Polymetamorphic evolution of pre-Alpidic basement relics in the external Hellenides, Greece. *Neues Jahrbuch für Mineralogie-Abhandlungen*, *181*(2), 147–172. <https://doi.org/10.1127/0077-7757/2005/0013>
- Gaudreau, É., Schneider, D. A., Lagroix, F., Cossette, É., & Grasemann, B. (2017). Controls and implications of anisotropy across a strain gradient within granulite, Serifos, Greece. *Journal of Geodynamics*, *105*, 11–26. <https://doi.org/10.1016/j.jog.2017.01.003>
- Gautier, P., Brun, J. P., & Jolivet, L. (1993). Structure and kinematics of upper Cenozoic extensional detachment on Naxos and Paros (Cyclades Islands, Greece). *Tectonics*, *12*(5), 1180–1194. <https://doi.org/10.1029/93TC01131>
- Gessner, K., Gallardo, L. A., Markwitz, V., Ring, U., & Thomson, S. N. (2013). What caused the denudation of the Menderes Massif: Review of crustal evolution, lithosphere structure, and dynamic topography in southwest Turkey. *Gondwana Research*, *24*(1), 243–274. <https://doi.org/10.1016/j.gr.2013.01.005>
- Gessner, K., Piazzolo, S., Güngör, T., Ring, U., Kröner, A., & Passchier, C. W. (2001a). Tectonic significance of deformation patterns in granitoid rocks of the Menderes nappes, Anatolide belt, southwest Turkey. *International Journal of Earth Sciences*, *89*(4), 766–780. <https://doi.org/10.1007/s005310000106>
- Gessner, K., Ring, U., Johnson, C., Hetzel, R., Passchier, C. W., & Güngör, T. (2001). An active bivergent rolling-hinge detachment system: Central Menderes metamorphic core complex in western Turkey. *Geology*, *29*(7), 611–614. [https://doi.org/10.1130/0091-7613\(2001\)029<0611:aabrdh>2.0.co;2](https://doi.org/10.1130/0091-7613(2001)029<0611:aabrdh>2.0.co;2)
- Godfriaux, I., & Ricou, L. E. (1991). Direction et sens de transport associés au cherriage symetamorphe sur l'Olympe. *Bulletin of the Geological Society of Greece*, *25*, 207–229.
- Godfriaux, Y., & Pichon, J. F. (1980). Sur l'importance des événements tectoniques et métamorphiques d'âge tertiaire en Thessalie septentrionale (L'Olympe, Ossa et Flamburon). *Annales Société Géologique Nord v.*, *99*, 367–376.
- Grasemann, B., Huet, B., Schneider, D. A., Rice, A. H. N., Lemonnier, N., & Tschegg, C. (2018). Miocene postorogenic extension of the Eocene synorogenic imbricated Hellenic subduction channel: New constraints from Milos (Cyclades, Greece). *GSA Bulletin*, *130*(1–2), 238–262. <https://doi.org/10.1130/b31731.1>
- Grasemann, B., Plan, L., Baroň, I., & Scholz, D. (2022b). Co-seismic deformation of the 2017 Mw 6.6 Bodrum–Kos earthquake in speleothems of Korakia Cave (Pserimos, Dodecanese, Greece). *Geomorphology*, *402*, 108137. <https://doi.org/10.1016/j.geomorph.2022.108137>
- Grasemann, B., Schneider, D. A., & Rogowitz, A. (2019). Back to normal: Direct evidence of the Cretan Detachment as a north-directed normal fault during the Miocene. *Tectonics*, *38*(8), 3052–3069. <https://doi.org/10.1029/2019tc005582>

- Grasemann, B., Schneider, D. A., Soukis, K., Roche, V., & Hubmann, B. (2022a). Paleogeographic position of the central Dodecanese Islands, southeastern Greece: The push-pull of Pelagonia. *GSA Bulletin*, 134(5–6), 1506–1528. <https://doi.org/10.1130/b36095.1>
- Grasemann, B., Schneider, D. A., Stöckli, D. F., & Iglseeder, C. (2012). Miocene divergent crustal extension in the Aegean: Evidence from the western Cyclades (Greece). *Lithosphere*, 4(1), 23–39. <https://doi.org/10.1130/1164.1>
- Hall, R., Audley-Charles, M. G., & Carter, D. J. (1984). The significance of Crete for the evolution of the Eastern Mediterranean. In J. E. Dixon & A. H. F. Robertson (Eds.), *The geological evolution of the Eastern Mediterranean* (Vol. 17, pp. 499–516). Geological Society, London, Special Publications.
- Henjes-Kunst, F., Altherr, R., Kreuzer, H., & Hansen, B. T. (1988). Disturbed U Th Pb systematics of young zircons and uranorhories: The case of the Miocene Aegean granitoids (Greece). *Chemical Geology: Isotope Geoscience section*, 73(2), 125–145. [https://doi.org/10.1016/0168-9622\(88\)90011-5](https://doi.org/10.1016/0168-9622(88)90011-5)
- Hetzl, R., Passchier, C. W., Ring, U., & Dora, O. O. (1995). Bivergent extension in orogenic belts: The Menderees massif (southwestern Turkey). *Geology*, 23(5), 455–458. [https://doi.org/10.1130/0091-7613\(1995\)023<0455:beiobt>2.3.co;2](https://doi.org/10.1130/0091-7613(1995)023<0455:beiobt>2.3.co;2)
- Hetzl, R., Zwingmann, H., Mulch, A., Gessner, K., Akal, C., Hampel, A., et al. (2013). Spatiotemporal evolution of brittle normal faulting and fluid infiltration in detachment fault systems: A case study from the Menderees Massif, western Turkey. *Tectonics*, 32(3), 364–376. <https://doi.org/10.1002/tect.20031>
- Iglseeder, C., Grasemann, B., Schneider, D. A., Petrakakis, K., Miller, C., Klötzli, U., et al. (2009). Tertiary I- and S-type plutonism on Serifos, western Cyclades, Greece. *Tectonophysics*, 473(1–2), 69–83. <https://doi.org/10.1016/j.tecto.2008.09.021>
- Işık, V., & Tekeli, O. (2001). Late orogenic crustal extension in the northern Menderees massif (western Turkey): Evidence for metamorphic core complex formation. *International Journal of Earth Sciences*, 89(4), 757–765. <https://doi.org/10.1007/s005310000105>
- Isik, V., Tekeli, O., & Seyitoglu, G. (2004). The ⁴⁰Ar/³⁹Ar age of extensional ductile deformation and granitoid intrusion in the northern Menderees core complex: Implications for the initiation of extensional tectonics in western Turkey. *Journal of Asian Earth Sciences*, 23(4), 555–566. <https://doi.org/10.1016/j.jseas.2003.09.001>
- Jacobshagen, V., Dürr, S., Kockel, F., Kopp, K. O., & Kowalczyk, G. (1978). Structure and geodynamic evolution of the Aegean region. In H. Cloos, D. Roeder, & K. Schmidt (Eds.), *Alps, Apennines, Hellenides: Stuttgart, Germany, Schweizerbart* (pp. 537–564).
- Jansen, J. B. H. (1977). The geology of Naxos, Greece. *Geology Geophysical Research*, 19/1, 1–100. IGMR, Athens.
- Jolivet, L., Arbaret, L., Le Pourhiet, L., Cheval-Garabédian, F., Roche, V., Rabillard, A., & Labrousse, L. (2021). Interactions of plutons and detachments: A comparison of Aegean and Tyrrhenian granitoids. *Solid Earth*, 12(6), 1357–1388. <https://doi.org/10.5194/se-12-1357-2021>
- Jolivet, L., & Brun, J. P. (2010). Cenozoic geodynamic evolution of the Aegean. *International Journal of Earth Sciences*, 99(1), 109–138. <https://doi.org/10.1007/s00531-008-0366-4>
- Jolivet, L., & Faccenna, C. (2000). Mediterranean extension and the Africa-Eurasia collision. *Tectonics*, 19(6), 1095–1106. <https://doi.org/10.1029/2000tc900018>
- Jolivet, L., Faccenna, C., Huet, B., Labrousse, L., Le Pourhiet, L., Lacombe, O., et al. (2013). Aegean tectonics: Strain localisation, slab tearing and trench retreat. *Tectonophysics*, 597, 1–33. <https://doi.org/10.1016/j.tecto.2012.06.011>
- Jolivet, L., Goffé, B., Monié, P., Truffert-Luxey, C., Patriat, M., & Bonneau, M. (1996). Miocene detachment in Crete and exhumation P-T-t paths of high-pressure metamorphic rocks. *Tectonics*, 15(6), 1129–1153. <https://doi.org/10.1029/96tc01417>
- Jolivet, L., Lecomte, E., Huet, B., Denèle, Y., Lacombe, O., Labrousse, L., et al. (2010). The North Cycladic detachment system. *Earth and Planetary Science Letters*, 289(1–2), 87–104. <https://doi.org/10.1016/j.epsl.2009.10.032>
- Jolivet, L., Rimmelé, G., Oberhänsli, R., Goffé, B., & Candan, O. (2004). Correlation of syn-orogenic tectonic and metamorphic events in the Cyclades, the Lycian nappes and the Menderees massif. Geodynamic implications. *Bulletin de la Société Géologique de France*, 175(3), 217–238. <https://doi.org/10.2113/175.3.217>
- Kahler, F. (1987). Fusuliniden-Faunen auf Chios, Kalymnos und Kos in der Aegaeis. Fusulinid faunas from the Aegean islands of Chios, Kalymnos and Kos. *Mitteilungen der Österreichischen Geologischen Gesellschaft*, 80, 287–323.
- Kalt, A., Altherr, R., & Ludwig, T. (1998). Contact metamorphism in pelitic rocks on the island of Kos (Greece, Eastern Aegean Sea): A test for the Na-in-cordierite thermometer. *Journal of Petrology*, 39(4), 663–688. <https://doi.org/10.1093/petrology/39.4.663>
- Kedar, L., Bond, C. E., & Muirhead, D. (2020). Carbon ordering in an aseismic shear zone: Implications for Raman geothermometry and strain tracking. *Earth and Planetary Science Letters*, 549, 116536. <https://doi.org/10.1016/j.epsl.2020.116536>
- Keller, J. (1969). Origin of rhyolites by anatexis melting of granitic crustal rocks. The example of rhyolitic pumice from the island of Kos (Aegean Sea). *Bulletin Volcanologique*, 33(3), 942–959. <https://doi.org/10.1007/bf02596758>
- Krahl, J., Kauffmann, G., Kozur, H., Richter, D., Förster, O., & Heinritzi, F. (1983). Neue Daten zur Biostratigraphie und zur tektonischen Lagerung der Phyllit-Gruppe und der Trypali-Gruppe auf der Insel Kreta (Griechenland). *Geologische Rundschau*, 72(3), 1147–1166. <https://doi.org/10.1007/bf01848358>
- Laskari, S., Soukis, K., Lozios, S., & Stockli, D. F. (2024). Switching from the top-NW backthrusting to top-SE post-orogenic deformation in the Aegean domain: Insights from the calcite microfabric and siliciclastic rocks of the Amorgos Unit (SE Cyclades, Greece). *Journal of Structural Geology*, 178, 105011. <https://doi.org/10.1016/j.jsg.2023.105011>
- Lips, A. L., Cassard, D., Sözbilir, H., Yılmaz, H., & Wijbrans, J. R. (2001). Multistage exhumation of the Menderees massif, western Anatolia (Turkey). *International Journal of Earth Sciences*, 89(4), 781–792. <https://doi.org/10.1007/s005310000101>
- Lister, G. S., Banga, G., & Feenstra, A. (1984). Metamorphic core complexes of Cordilleran type in the Cyclades, Aegean Sea, Greece. *Geology*, 12(4), 221–225. [https://doi.org/10.1130/0091-7613\(1984\)12<221:MCCOCT>2.0.CO;2](https://doi.org/10.1130/0091-7613(1984)12<221:MCCOCT>2.0.CO;2)
- Marinos, G., & Petraschek, W. E. (1956). Laurium. *Geological and Geophysical Research* (Special Issue 1–247).
- Melidonis, N. G. (1980). The geological structure and mineral deposits of Tinos island (Cyclades, Greece). In *The geology of Greece* (Vol. 13, pp. 0–80). IGME.
- Mezger, K., Altherr, R., Okrusch, M., Henjes-Kunst, F., & Kreuzer, H. (1985). Genesis of acid/basic rock associations: A case study the Kallithea intrusive complex, Samos, Greece. *Contributions to Mineralogy and Petrology*, 90(4), 353–366. <https://doi.org/10.1007/BF00384714>
- Mountrakis, D. (1986). The Pelagonian zone in Greece: A polyphase-deformed fragment of the Cimmerian continent and its role in the geotectonic evolution of the eastern Mediterranean. *The Journal of Geology*, 94(3), 335–347. <https://doi.org/10.1086/629033>
- Muirhead, D. K., Kedar, L., Schito, A., Corrado, S., Bond, C. E., & Romano, C. (2021). Raman spectral shifts in naturally faulted rocks. *Geochemistry, Geophysics, Geosystems*, 22(10), e2021GC009923. <https://doi.org/10.1029/2021GC009923>
- Orombelli, G., Lozej, G. P., Rossi, L. A., & Desio, A. (1967). Preliminary notes on the geology of the Datça peninsula (SW Turkey). *Atti della Accademia Nazionale dei Lincei*, 8(42), 830–841.
- Papanikolaou, D. (2013). Tectonostratigraphic models of the Alpine terranes and subduction history of the Hellenides. *Tectonophysics*, 595, 1–24. <https://doi.org/10.1016/j.tecto.2012.08.008>
- Papanikolaou, D. (2021). *The geology of Greece*. Springer Nature. <https://doi.org/10.1007/978-3-030-60731-9>

- Papanikolaou, D., & Demirtasli, E. (1987). Geological correlations between the alpine segments of the Hellenides-Balkanides and Taurides-Pontides. In H. W. Flügel, F. P. Sassi, & P. Grecula (Eds.), *Pre-Variscan and Variscan events in the alpine Mediterranean Mountain Belts: Bratislava* (pp. 387–396). Mineralia Slovaca.
- Papanikolaou, D., & Nomikou, P. V. (1998). *The Palaeozoic of Kos: A low grade metamorphic unit of the basement of the external Hellenides Terrane* (pp. 155–166). IGCP Project No 276, 6.
- Parra, T., Vidal, O., & Jolivet, L. (2002). Relation between the intensity of deformation and retrogression in blueschist metapelites of Tinos Island (Greece) evidenced by chlorite–mica local equilibria. *Lithos*, 63(1–2), 41–66. [https://doi.org/10.1016/S0024-4937\(02\)00115-9](https://doi.org/10.1016/S0024-4937(02)00115-9)
- Patzak, M., Okrusch, M., & Kreuzer, H. (1994). The Akrotiri Unit on the island of Tinos, Cyclades, Greece: Witness to a lost terrane of Late Cretaceous age. *Neues Jahrbuch für Geologie und Paläontologie-Abhandlungen*, 194(2–3), 211–252. <https://doi.org/10.1127/njgpa/194/1994/211>
- Pe-Piper, G., Piper, D. J. W., & Perissoratis, C. (2005). Neotectonics and the Kos Plateau Tuff eruption of 161 ka, South Aegean arc. *Journal of Volcanology and Geothermal Research*, 139(3–4), 315–338. <https://doi.org/10.1016/j.jvolgeores.2004.08.014>
- Piromallo, C., & Morelli, A. (2003). P wave tomography of the mantle under the Alpine-Mediterranean area. *Journal of Geophysical Research*, 108(B2), 2065. <https://doi.org/10.1029/2002JB001757>
- Platt, J. P. (1986). Dynamics of orogenic wedges and the uplift of high-pressure metamorphic rocks. *Geological Society of America Bulletin*, 97(9), 1037–1053. [https://doi.org/10.1130/0016-7606\(1986\)97<1037:doowat>2.0.co;2](https://doi.org/10.1130/0016-7606(1986)97<1037:doowat>2.0.co;2)
- Pourteau, A., Sudo, M., Candan, O., Lanari, P., Vidal, O., & Oberhänsli, R. (2013). Neotethys closure history of Anatolia: Insights from ⁴⁰Ar–³⁹Ar geochronology and P–T estimation in high-pressure metasedimentary rocks. *Journal of Metamorphic Geology*, 31(6), 585–606. <https://doi.org/10.1111/jmg.12034>
- Rabillard, A., Jolivet, L., Arbaret, L., Bessière, E., Laurent, V., Menant, A., et al. (2018). Synextensional granitoids and detachment systems within Cycladic metamorphic core complexes (Aegean Sea, Greece): Toward a regional tectonomagmatic model. *Tectonics*, 37(8), 2328–2362. <https://doi.org/10.1029/2017TC004697>
- Rimmelé, G., Jolivet, L., Oberhänsli, R., & Goffé, B. (2003). Deformation history of the high-pressure Lycian Nappes and implications for tectonic evolution of SW Turkey. *Tectonics*, 22(2). <https://doi.org/10.1029/2001TC901041>
- Rimmelé, G., Parra, T., Goffé, B., Oberhänsli, R., Jolivet, L., & Candan, O. (2005). Exhumation paths of high-pressure–low-temperature metamorphic rocks from the Lycian Nappes and the Menderes Massif (SW Turkey): A multi-equilibrium approach. *Journal of Petrology*, 46(3), 641–669. <https://doi.org/10.1093/petrology/egh092>
- Ring, U., Gessner, K., Güngör, T., & Passchier, C. W. (1999). The Menderes Massif of western Turkey and the Cycladic Massif in the Aegean—Do they really correlate? *Journal of the Geological Society*, 156(1), 3–6. <https://doi.org/10.1144/gsjgs.156.1.0003>
- Ring, U., Gessner, K., & Thomson, S. (2017). Variations in fault-slip data and cooling history reveal corridor of heterogeneous backarc extension in the eastern Aegean Sea region. *Tectonophysics*, 700–701, 108–130. <https://doi.org/10.1016/j.tecto.2017.02.013>
- Ring, U., Glodny, J., Will, T., & Thomson, S. (2010). The Hellenic subduction system. High-pressure metamorphism, exhumation, normal faulting, and large-scale extension. *Annual Review of Earth and Planetary Sciences*, 38(1), 45–76. <https://doi.org/10.1146/annurev.earth.050708.170910>
- Ring, U., Johnson, C., Hetzel, R., & Gessner, K. (2003). Tectonic denudation of a Late Cretaceous–Tertiary collisional belt: Regionally symmetric cooling patterns and their relation to extensional faults in the Anatolide belt of western Turkey. *Geological Magazine*, 140(4), 421–441. <https://doi.org/10.1017/S0016756803007878>
- Ring, U., Layer, P. W., & Reischmann, T. (2001). Miocene high-pressure metamorphism in the Cyclades and Crete, Aegean Sea, Greece: Evidence for large-magnitude displacement on the Cretan detachment. *Geology*, 29(5), 395–398. [https://doi.org/10.1130/0091-7613\(2001\)029<0395:MHPMIT>2.0.CO;2](https://doi.org/10.1130/0091-7613(2001)029<0395:MHPMIT>2.0.CO;2)
- Robert, U., Foden, J., & Varne, R. (1992). The Dodecanese Province, SE Aegean: A model for tectonic control on potassic magmatism. *Lithos*, 28(3–6), 241–260. [https://doi.org/10.1016/0024-4937\(92\)90009-n](https://doi.org/10.1016/0024-4937(92)90009-n)
- Roche, V., Conand, C., Jolivet, L., & Augier, R. (2018). Tectonic evolution of Leros (Dodecanese, Greece) and correlations between the Aegean Domain and the Menderes Massif. *Journal of the Geological Society*, 175(5), 836–849. <https://doi.org/10.1144/jgs2018-028>
- Roche, V., Jolivet, L., Papanikolaou, D., Bozkurt, E., Menant, A., & Rimmelé, G. (2019). Slab fragmentation beneath the Aegean/Anatolia transition zone: Insights from the tectonic and metamorphic evolution of the Eastern Aegean region. *Tectonophysics*, 754, 101–129. <https://doi.org/10.1016/j.tecto.2019.01.016>
- Salaün, G., Pedersen, H. A., Paul, A., Farra, V., Karabulut, H., Hatzfeld, D., et al. (2012). High-resolution surface wave tomography beneath the Aegean-Anatolia region: Constraints on upper-mantle structure. *Geophysical Journal International*, 190(1), 406–420. <https://doi.org/10.1111/j.1365-246X.2012.05483.x>
- Scherreiks, R., Meléndez, G., BouDagher-Fadel, M., Fermeli, G., & Bosence, D. (2014). Stratigraphy and tectonics of a time-transgressive ophiolite obduction onto the eastern margin of the Pelagonian platform from Late Bathonian until Valanginian time, exemplified in northern Evvoia, Greece. *International Journal of Earth Sciences*, 103(8), 2191–2216. <https://doi.org/10.1007/s00531-014-1036-3>
- Schmid, S. M., Fügenschuh, B., Kounov, A., Mañenco, L., Nievergelt, P., Oberhänsli, R., et al. (2020). Tectonic units of the Alpine collision zone between Eastern Alps and western Turkey. *Gondwana Research*, 78, 308–374. <https://doi.org/10.1016/j.gr.2019.07.005>
- Schneider, D. A., Grasmann, B., Lion, A., Soukis, K., & Draganits, E. (2018). Geodynamic significance of the Santorini detachment system (Cyclades, Greece). *Terra Nova*, 30(6), 414–422. <https://doi.org/10.1111/ter.12357>
- Seyitoğlu, G., Işık, V., & Cemen, I. (2004). Complete Tertiary exhumation history of the Menderes massif, western Turkey: An alternative working hypothesis. *Terra Nova*, 16(6), 358–364. <https://doi.org/10.1111/j.1365-3121.2004.00574.x>
- Shaked, Y., Avigad, D., & Garfunkel, Z. (2000). Alpine high-pressure metamorphism at the Almyropotamos window (southern Evia, Greece). *Geological Magazine*, 137(4), 367–380. <https://doi.org/10.1017/s001675680000426x>
- Smith, P. E., York, D., Chen, Y., & Evensen, N. M. (1996). Single crystal ⁴⁰Ar–³⁹Ar dating of a Late Quaternary paroxysm on Kos, Greece: Concordance of terrestrial and marine ages. *Geophysical Research Letters*, 23(21), 3047–3050. <https://doi.org/10.1029/96gl02759>
- Soder, C., Altherr, R., & Romer, R. L. (2016). Mantle metasomatism at the edge of a retreating subduction zone: Late Neogene lamprophyres from the Island of Kos, Greece. *Journal of Petrology*, 57(9), 1705–1728. <https://doi.org/10.1093/petrology/egw054>
- Stiwe, K. (2007). *Geodynamics of the lithosphere* (p. 493). Springer.
- Triantaphyllis, M. B., & Mavrides, A. N. (1998). *Geological map of Greece: Eastern Kos Sheet*. Institute of Geology and Mineral Exploration (IGME), scale 1:50,000.
- Tselepidis, V., & Carras, N. (2013). *Internal report on the results of the field-work on Kalymnos Island, Athens, Greece* (p. 13). Institute of Geological and Mining Exploration.
- Urai, J. L., Schuiling, R. D., & Jansen, J. B. H. (1990). Alpine deformation on Naxos (Greece). *Geological Society, London, Special Publications*, 54(1), 509–522. <https://doi.org/10.1144/gsl.sp.1990.054.01.47>

- van Hinsbergen, D. J. J., & Boekhout, F. (2009). Neogene brittle detachment faulting on Kos (E Greece): Implications for a southern break-away fault of the Menderes metamorphic core complex (western Turkey). *Geological Society, London, Special Publications*, 311(1), 311–320. <https://doi.org/10.1144/sp311.12>
- van Hinsbergen, D. J. J., Hafkenscheid, E., Spakman, W., Meulenkamp, J. E., & Wortel, R. (2005). Nappe stacking resulting from subduction of oceanic and continental lithosphere below Greece. *Geology*, 33(4), 325–328. <https://doi.org/10.1130/G20878.1>
- Wijbrans, J. R., & McDougall, I. (1988). Metamorphic evolution of the Attic Cycladic Metamorphic Belt on Naxos (Cyclades, Greece) utilizing $^{40}\text{Ar}/^{39}\text{Ar}$ age spectrum measurements. *Journal of Metamorphic Geology*, 6(5), 571–594. <https://doi.org/10.1111/j.1525-1314.1988.tb00441.x>
- Willmann, R. (1983). Neogen und jungtertiäre Entwicklung der Insel Kos (Ägäis, Griechenland). *Geologische Rundschau*, 72(3), 815–860. <https://doi.org/10.1007/bf01848345>

References From the Supporting Information

- Best, M., Christiansen, E., Deino, A., Grommé, C., & Tingey, D. (1995). Correlation and emplacement of a large, zoned, discontinuously exposed ash flow sheet; the $^{40}\text{Ar}/^{39}\text{Ar}$ chronology, paleomagnetism, and petrology of the Pahrangat Formation, Nevada. *Journal of Geophysical Research*, 100(B12), 24593–24609. <https://doi.org/10.1029/95jb01690>
- Dazé, A., Lee, J., & Villeneuve, M. (2003). An intercalibration study of the Fish Canyon sanidine and biotite $^{40}\text{Ar}/^{39}\text{Ar}$ standards and some comments on the age of the Fish Canyon Tuff. *Chemical Geology*, 199(1–2), 111–127. [https://doi.org/10.1016/s0009-2541\(03\)00079-2](https://doi.org/10.1016/s0009-2541(03)00079-2)
- Kuiper, K., Deino, A., Hilgen, F., Krijgsman, W., Renne, R., & Wijbrans, J. (2008). Synchronizing rock clocks of Earth history. *Science*, 320(5875), 500–504. <https://doi.org/10.1126/science.1154339>
- Lahfid, A., Beyssac, O., Deville, E., Negro, F., Chopin, C., & Goffé, B. (2010). Evolution of the Raman spectrum of carbonaceous material in low-grade metasediments of the Glarus Alps (Switzerland). *Terra Nova*, 22(5), 354–360. <https://doi.org/10.1111/j.1365-3121.2010.00956.x>
- Pasteris, J. D., & Wopenka, B. (1991). Raman spectra of graphite as indicators of degree of metamorphism. *The Canadian Mineralogist*, 29(1), 1–9.
- Renne, P., & Norman, E. (2001). Determination of the half-life of ^{40}Ar by mass spectrometry. *Physical Review C*, 63(3), 047302. <https://doi.org/10.1103/physrevc.63.047302>
- Renne, P., Swisher, C., Deino, A., Karner, D., Owens, T., & DePaolo, D. (1998). Intercalibration of standards, absolute ages and uncertainties in $^{40}\text{Ar}/^{39}\text{Ar}$ dating. *Chemical Geology*, 145(1–2), 117–152. [https://doi.org/10.1016/s0009-2541\(97\)00159-9](https://doi.org/10.1016/s0009-2541(97)00159-9)
- Roddick, J. (1983). High precision intercalibration of $^{40}\text{Ar}/^{39}\text{Ar}$ standards. *Geochimica et Cosmochimica Acta*, 47(5), 887–898. [https://doi.org/10.1016/0016-7037\(83\)90154-0](https://doi.org/10.1016/0016-7037(83)90154-0)
- Spell, T., & McDougall, I. (2003). Characterization and calibration of $^{40}\text{Ar}/^{39}\text{Ar}$ dating standards. *Chemical Geology*, 198(3–4), 189–211. [https://doi.org/10.1016/s0009-2541\(03\)00005-6](https://doi.org/10.1016/s0009-2541(03)00005-6)
- Steiger, R., & Jäger, E. (1977). Subcommittee on geochronology: Convention on the use of decay constants in geo- and cosmochronology. *Earth and Planetary Science Letters*, 36(3), 359–362. [https://doi.org/10.1016/0012-821x\(77\)90060-7](https://doi.org/10.1016/0012-821x(77)90060-7)
- Wopenka, B., & Pasteris, J. D. (1993). Structural characterization of kerogens to granulite-facies graphite: Applicability of Raman microprobe spectroscopy. *American Mineralogist*, 78(5–6), 533–557.